On the generalisation of the mixture fraction to a monotonic mixing-describing variable for the flamelet formulation of spray flames

Benedetta Franzelli, Aymeric Vié, Matthias Ihme

Combustion Theory and Modelling
Vol. 00, No. 00, Month 200x, 1–33

RESEARCH ARTICLE

On the generalization of the mixture fraction to a monotonic mixing-describing variable for the flamelet formulation of spray flames

Benedetta Franzelli[a,b,⋆] Aymeric Vié[a,†,∗] and Matthias Ihme[a,‡]
[a] *Department of Mechanical Engineering, Stanford University, Stanford, CA 94305, USA*
[b] *Laboratoire EM2C, CNRS, CentraleSupelec, Chatenay-Malabry, 92295, France*
(*Received 00 Month 200x; final version received 00 Month 200x*)

Spray flames are complex combustion configurations that require the consideration of competing processes between evaporation, mixing and chemical reactions. The classical mixture-fraction formulation, commonly employed for the representation of gaseous diffusion flames, cannot be used for spray flames due to its non-monotonicity. This is a consequence of the presence of an evaporation source term in the corresponding conservation equation. By addressing this issue, a new mixing-describing variable, called effective composition variable η, is defined to enable the general analysis of spray-flame structures in composition space. This quantity combines the gaseous mixture fraction Z_g and the liquid-to-gas mass ratio Z_l, and is defined as: $\mathrm{d}\eta = \sqrt{(\mathrm{d}Z_g)^2 + (\mathrm{d}Z_l)^2}$. This new expression reduces to the classical mixture-fraction definition for gaseous systems, thereby ensuring consistency. The versatility of this new expression is demonstrated in application to the analysis of counterflow spray flames. Following this analysis, the effective composition variable η is employed for the derivation of a spray-flamelet formulation. The consistent representation in both effective-composition space and physical space is guaranteed by construction and the feasibility of solving the resulting spray-flamelet equation in this newly defined composition space is demonstrated numerically. A model for the scalar dissipation rate is proposed to close the derived spray-flamelet equations.The laminar one-dimensional counterflow spray flamelet equations are numerically solved in the η-space and compared to the physical-space solutions. It is shown that the hysteresis and bifurcation characterizing the flame structure response to variations of droplet diameter and strain rate are correctly reproduced by the proposed composition-space formulation.

Keywords: Laminar counterflow spray flames; Flamelet formulation; Mixture fraction; Effective composition; Bifurcation; Hysteresis

1. Introduction

Motivated by the utilization of liquid fuels for transportation and propulsion systems, considerable progress has been made on the analysis of spray flames [1–6]. While gaseous diffusion flames are characterized by the competition between scalar mixing and chemistry, spray flames require the continuous supply of gaseous fuel via evaporation and transport to the reaction zone to sustain combustion. Because of this complexity, the investigation of spray flames in canonical combustion configurations, such as mixing layers, coflow and counterflow flames, represents a viable approach to obtain physical insight into the behavior of spray flames [7–11].

⋆ Email: benedetta.franzelli@ecp.fr
† Current Address: Laboratoire EM2C, CNRS, CentraleSupelec, Chatenay-Malabry, 92295, France
∗ Email: aymeric.vie@ecp.fr
‡ Corresponding author. Email: mihme@stanford.edu; Phone: +1(650) 724-3730

Counterflow spray flames have been the subject of intensive research, and considerable numerical and experimental studies have been performed by considering laminar conditions [7, 12–17]. Theoretical investigations provided understanding about underlying physical processes, flame stabilization and extinction processes of spray flames [11, 18–20]. Experiments in counterflow flames have been performed to examine extinction behavior of mono- and polydisperse spray flames through strain variation and vortex interaction [21, 22]. More recently, bistable flame structures of laminar flames were considered for examining the bifurcation in three-dimensional turbulent counterflow spray flames [23]. As such, these studies demonstrated that the structure of spray flames is of fundamental relevance for a wide range of operating regimes.

In the context of laminar gaseous diffusion flames, the flame structure is typically examined in composition space by introducing the gaseous mixture fraction Z_g as an independent variable [24]. For a given strain rate, the flame structure is then fully parameterized in terms of the gaseous mixture composition, providing a unique mapping between physical and composition space. This mixture-fraction formulation is also used in turbulent combustion models, enabling the representation of the turbulence-chemistry interaction through presumed probability density function models [25, 26]. Another significant advantage of a mixture-fraction representation arises from the computationally efficient solution of the resulting flamelet equations in composition state. Therefore, extending the mixture-fraction concept to spray flames is desirable and enables the utilization of analysis tools that have been developed for gaseous flames.

Unfortunately, this extension is non-trivial, since the classical gaseous mixture-fraction definition looses its monotonicity due to evaporation [27, 28]. With the exception of pre-vaporized flames and other simplifying assumptions, the structure of spray flames cannot be studied in the classical mixture-fraction space.

Previous works have dealt with the extension of the mixture fraction definition to spray flames. Sirignano [29] and Bilger [30] have investigated the definition of mixing-describing variables for two-phase combustion. Their works apply to the characterization of the mixture evolution from the droplet (or ligament) surface to the far field. Such an approach is only applicable if the diffusive layer around each droplet is small compared to the droplet interspacing. In cases where the droplet interspacing is too small compared to flame and diffusive scales, a mesoscopic point of view should be adopted and a continuum representation is required with regard to the mixture-fraction field [3]. Although Bilger's approach is able to recover the mesoscopic limit, the detailed representation of these scales is computationally expensive. In this scenario, extending the mixture fraction concept to spray flames is not straightforward. This issue was mentioned in [31], and a total mixture fraction was introduced to account for both gas and liquid contributions. Luo et al. [32] extended the classical mixture fraction flamelet transformation to spray flames, but only for pre-vaporized conditions that serve the definition of the boundary conditions for the gaseous flamelet equations. Olguin and Gutheil [27, 33], Greenberg et al. [11, 18–20] and Maionchi and Fachini [34] directly solved the spray flame equations in physical space and subsequently represented the flame structure in the Z_g-space; for example by separating the purely gaseous region of the flame from the evaporation zone [27, 33]. However, due to the non-monotonicity, the classical gaseous definition cannot be used to solve the spray flamelet equations in composition space.

By addressing these issues, this work proposes a new composition-space variable that enables the description of spray flames. The key idea for this formulation consists in identifying a monotonic representation of a mixing-describing coordinate

for spray flames. This new coordinate, referred to as effective composition variable η, is both useful for analyzing the flame structure and for effectively solving the corresponding spray flamelet equations. In addition, the effective composition variable η is defined in such a way that it extends the classical flamelet formulation for gaseous diffusion systems [24, 35–37], thereby ensuring consistency. Compared to a non-monotonic definition, the use of the proposed effective composition variable for spray flames exhibits the following advantages:

- it allows a mathematical well-posed definition of the transformation from physical to composition space, thereby providing a theoretical foundation for one-dimensional laminar spray flamelet formulations.
- it enables the representation of the system in composition space, eliminating the explicit dependence on the spatial coordinate, thereby providing a computationally more efficient solution.
- it allows the analysis of spray flames in analogy to the work on gaseous flames based on a mixture-fraction formulation [36, 38].
- it provides direct insight of the flame structure without any additional postprocessing that is otherwise required, for example, when using the classical gaseous Z_g-space.

The remainder of this paper is organized as follows. The spray-flamelet equations in physical space and composition space are presented in Sec. 2. The effective composition formulation and its mathematical properties are discussed in Sec. 3. The versatility of this effective composition space formulation is demonstrated by considering two applications. The first application (Sec. 4) is concerned with the analysis of the spray-flame structure in composition space. The second application concerns the use of η to directly solve the spray-flame system in composition space. For this, the spray-flamelet equations in η-space are formulated in Sec. 5, and a closure model for the scalar dissipation rate is proposed in App. C. Comparisons of simulation results with solutions obtained in physical space are performed and different levels of model approximations are assessed. It is shown that the proposed formulation is able to reproduce the bifurcation and hysteresis, characterizing the flame-structure response to strain-rate and droplet-diameter variations. The paper finishes by offering conclusions and perspectives.

2. Governing equations

In the present work, we consider a mono-disperse spray flame in a counterflow configuration, and the governing equations are formulated in an Eulerian framework. In this configuration, fresh air is injected against a stream consisting of a fuel spray and pure air. Consistent with the classical analysis of gaseous flames, the following assumptions are invoked [24, 35, 37]:

(1) Steady-state solution and low-Mach number limit.
(2) Unconfined flame and constant thermodynamic pressure.
(3) Single-component fuel.
(4) Unity Lewis number. Equal but not necessarily constant diffusivities are assumed for all chemical species and temperature: $D_k = D_{th} = \lambda/(\rho c_p) \equiv D$. Ficks' law without velocity correction is used for diffusion velocities [37].
(5) Calorically perfect gas: $c_{p,k} = c_p =$ constant.

In this context, it is noted that the composition variable and formulation proposed in this paper are not restricted to these assumptions and can equally be extended

in analogy to the theory for gaseous flames, and guidance on the extension to non-unity Lewis numbers is provided in App. E.

Under these assumptions, the transport equations for gaseous and liquid phases in physical space are introduced next. From this, we derive the general spray flamelet formulation, which serves as foundation for the following analysis.

2.1 *Spray flame equations in physical space*

Gas-phase equations The gaseous phase is described by the transport equations for momentum, species mass fractions, temperature and mixture fraction Z_g:

$$\rho u_i \frac{\partial u_j}{\partial x_i} = \frac{\partial}{\partial x_i}\left(\mu \frac{\partial u_j}{\partial x_i}\right) - \frac{\partial p}{\partial x_j} + (u_j - u_{l,j})\dot{m} - f_j \ , \tag{1a}$$

$$\rho u_i \frac{\partial Y_k}{\partial x_i} = \frac{\partial}{\partial x_i}\left(\rho D \frac{\partial Y_k}{\partial x_i}\right) + \dot{\omega}_k + (\delta_{kF} - Y_k)\dot{m} \ , \qquad \text{for } k = 1, \ldots, N_s \tag{1b}$$

$$\rho u_i \frac{\partial T}{\partial x_i} = \frac{\partial}{\partial x_i}\left(\rho D \frac{\partial T}{\partial x_i}\right) + \dot{\omega}_T + \dot{m}\left(T_l - T - \frac{q}{c_p}\right) \ , \tag{1c}$$

$$\rho u_i \frac{\partial Z_g}{\partial x_i} = \frac{\partial}{\partial x_i}\left(\rho D \frac{\partial Z_g}{\partial x_i}\right) + (1 - Z_g)\dot{m} \ , \tag{1d}$$

where ρ is the density, p is the pressure, and u_j is the j^{th} component of the velocity vector. The production rate of species k is denoted by $\dot{\omega}_k$, $\dot{\omega}_T = -\sum_{k=1}^{N_s} \dot{\omega}_k W_k h_k / c_p$ is the heat released by combustion, W_k is the molecular weight of species k, h_k is the sensible and chemical enthalpy of species k, c_p is the heat capacity of the gaseous mixture, q is the ratio between heat transfer and mass transfer rates from the gas to each droplet, δ_{ij} is the Kronecker delta, and N_s is the total number of species. The total mass vaporization rate is $\dot{m}$, T is the temperature, μ is the dynamic viscosity of the gas mixture, and f_j is the jth component of the drag force, which is here modeled by the Stokes law [39]. Subscript l is used to identify quantities of the liquid phase and the subscript F refers to the fuel. The gaseous non-normalized mixture fraction is here formulated with respect to the carbon-containing species [40]:

$$Z_g = \frac{W_F}{n_{CF} W_C} \sum_{k=1}^{N_s} n_{C,k} \frac{Y_k W_C}{W_k} \ , \tag{2}$$

where Y_k is the mass fraction of species k, $n_{C,k}$ is the number of carbon atoms in species k and W_C is the carbon molecular weight.

Liquid-phase equations As we are considering spray combustion, the liquid phase is composed of a set of droplets. The following assumptions are made:

- Monodisperse/Monokinetic/Mono-temperature spray: all the droplets in the same vicinity have the same diameter, velocity and temperature.
- Dilute spray: the spray volume fraction is negligible compared to that of the gas phase. Consequently, the gas phase volume fraction is assumed to be one in the gas phase equations.
- The only external force acting on the particle trajectory is the drag force.
- One-way coupling and no droplet/droplet interaction or secondary break-up are

considered.

Consequently, the balance equations for the total liquid mass, the individual droplet mass, the liquid momentum, and the enthalpy of the liquid phase $dh_l = c_l dT_l$ read as [7]:

$$\frac{\partial(\rho_l \alpha_l u_{l,i})}{\partial x_i} = -\dot{m} \ , \tag{3a}$$

$$n_l u_{l,i} \frac{\partial m_d}{\partial x_i} = -\dot{m} \ , \tag{3b}$$

$$\frac{\partial(\rho_l \alpha_l u_{l,i} u_{l,j})}{\partial x_i} = -f_j - \dot{m} u_{l,j} \ , \tag{3c}$$

$$\frac{\partial(\rho_l \alpha_l u_{l,i} h_l)}{\partial x_i} = -\dot{m}(h_l - q + L_v) \ , \tag{3d}$$

where $\alpha_l = n_l \pi d^3/6$ is the liquid volume fraction, $m_d = \rho_l \pi d^3/6$ is the individual droplet mass, ρ_l is the liquid density, d is the droplet diameter, n_l is the liquid droplet number density, c_l is the liquid heat capacity, and L_v is the latent heat of evaporation. By introducing the liquid-to-gas mass ratio:

$$Z_l = \frac{\alpha_l \rho_l}{(1-\alpha_l)\rho} \approx \frac{\alpha_l \rho_l}{\rho}, \tag{4}$$

Eqs. (3) can be written in non-conservative form:

$$\rho u_i \frac{\partial Z_l}{\partial x_i} = \frac{\partial[\rho(u_i - u_{l,i}) Z_l]}{\partial x_i} - \dot{m}\,(1 + Z_l) \ , \tag{5a}$$

$$\rho u_i \frac{\partial m_d}{\partial x_i} = -\frac{\rho}{n_l}\dot{m} + \frac{\partial[\rho(u_i - u_{l,i}) m_d]}{\partial x_i} \ , \tag{5b}$$

$$\rho u_i \frac{\partial(u_{l,j} Z_l)}{\partial x_i} = \frac{\partial[\rho u_{l,j}(u_i - u_{l,i}) Z_l]}{\partial x_i} - f_j + \dot{m} u_{l,j}\,(1 + Z_l) \ , \tag{5c}$$

$$\rho u_i \frac{\partial(Z_l h_l)}{\partial x_i} = \frac{\partial[\rho h_l (u_i - u_{l,i}) Z_l]}{\partial x_i} - \dot{m}(1 + Z_l) h_l + \dot{m}(L_v - q) \ . \tag{5d}$$

In the following, Eqs. (1) and (5) are used to derive the spray flamelet equations.

2.2 *General spray flamelet formulation*

The general spray flamelet equations can be derived in analogy to the analysis for counterflow gaseous flames [24]. The physical coordinate along the flame-normal direction can be expressed in terms of a generic variable ζ, which is assumed to monotonically increase from the oxidizer side to the spray injection side. By introducing the transformation from physical space to composition space, $(x_1, x_2, x_3) \rightarrow (\zeta(x_i), \zeta_2, \zeta_3)$, all spatial derivatives can be written as:

$$\frac{\partial}{\partial x_1} = \frac{\partial \zeta}{\partial x_1}\frac{\partial}{\partial \zeta} \ , \tag{6a}$$

$$\frac{\partial}{\partial x_i} = \frac{\partial}{\partial \zeta_i} + \frac{\partial \zeta}{\partial x_i}\frac{\partial}{\partial \zeta} \qquad \text{for } i = 2, 3. \tag{6b}$$

It is important to note that the strict monotonicity of the quantity ζ is essential to guarantee the mathematical well-posedness of the transformation in Eq. (6), which is not defined for $\partial_{x_i}\zeta{=}0$.

Peters assumed [24] that derivatives along the ζ-direction are much larger compared to those along the tangential directions (ζ_2 and ζ_3). By neglecting these high-order contributions, the following operators are obtained:

$$\rho u_i \frac{\partial \phi}{\partial x_i} = \Xi_\zeta \frac{\partial \phi}{\partial \zeta} \,, \tag{7a}$$

$$\frac{\partial}{\partial x_i}\left(\rho D \frac{\partial \phi}{\partial x_i}\right) = \frac{\partial \phi}{\partial \zeta}\left[\frac{\rho D}{2}\frac{\partial}{\partial \zeta}\left(\frac{\chi_\zeta}{2D}\right) + \frac{\chi_\zeta}{2D}\frac{\partial \rho D}{\partial \zeta}\right] + \frac{\rho \chi_\zeta}{2}\frac{\partial^2 \phi}{\partial \zeta^2} \,, \tag{7b}$$

$$\frac{\partial}{\partial x_i}\left(\mu \frac{\partial \phi}{\partial x_i}\right) = \frac{\partial \phi}{\partial \zeta}\left[\frac{\mu}{2}\frac{\partial}{\partial \zeta}\left(\frac{\chi_\zeta}{2D}\right) + \frac{\chi_\zeta}{2D}\frac{\partial \mu}{\partial \zeta}\right] + \frac{\mu}{D}\frac{\chi_\zeta}{2}\frac{\partial^2 \phi}{\partial \zeta^2} \,, \tag{7c}$$

where

$$\Xi_\zeta = \rho u_i \frac{\partial \zeta}{\partial x_i} \tag{8}$$

is the material derivative of ζ, and χ_ζ is the scalar dissipation of the variable ζ:

$$\chi_\zeta = 2D \frac{\partial \zeta}{\partial x_i}\frac{\partial \zeta}{\partial x_i} \,. \tag{9}$$

With this, the equations for the gas phase, Eqs. (1), can be rewritten as:

$$\frac{\mathrm{d}u_j}{\mathrm{d}\zeta}\left(\Xi_\zeta - \frac{\mu}{2}\frac{\mathrm{d}}{\mathrm{d}\zeta}\left(\frac{\chi_\zeta}{2D}\right) - \frac{\chi_\zeta}{2D}\frac{\mathrm{d}\mu}{\mathrm{d}\zeta}\right) = \frac{\mu}{D}\frac{\chi_\zeta}{2}\frac{\mathrm{d}^2 u_j}{\mathrm{d}\zeta^2} + (u_j - u_{l,j})\dot{m} - f_j + J_j\frac{\mathrm{d}p}{\mathrm{d}\zeta} \,, \tag{10a}$$

$$\frac{\mathrm{d}Y_k}{\mathrm{d}\zeta}\left(\Xi_\zeta - \frac{\rho D}{2}\frac{\mathrm{d}}{\mathrm{d}\zeta}\left(\frac{\chi_\zeta}{2D}\right) - \frac{\chi_\zeta}{2D}\frac{\mathrm{d}(\rho D)}{\mathrm{d}\zeta}\right) = \frac{\rho\chi_\zeta}{2}\frac{\mathrm{d}^2 Y_k}{\mathrm{d}\zeta^2} + (\delta_{kF} - Y_k)\dot{m} + \dot{\omega}_k, \tag{10b}$$

$$\frac{\mathrm{d}T}{\mathrm{d}\zeta}\left(\Xi_\zeta - \frac{\rho D}{2}\frac{\mathrm{d}}{\mathrm{d}\zeta}\left(\frac{\chi_\zeta}{2D}\right) - \frac{\chi_\zeta}{2D}\frac{\mathrm{d}(\rho D)}{\mathrm{d}\zeta}\right) = \frac{\rho\chi_\zeta}{2}\frac{\mathrm{d}^2 T}{\mathrm{d}\zeta^2} + \dot{m}\left(T_l - T - \frac{q}{c_p}\right) + \dot{\omega}_T, \tag{10c}$$

$$\frac{\mathrm{d}Z_g}{\mathrm{d}\zeta}\left(\Xi_\zeta - \frac{\rho D}{2}\frac{\mathrm{d}}{\mathrm{d}\zeta}\left(\frac{\chi_\zeta}{2D}\right) - \frac{\chi_\zeta}{2D}\frac{\mathrm{d}(\rho D)}{\mathrm{d}\zeta}\right) = \frac{\rho\chi_\zeta}{2}\frac{\mathrm{d}^2 Z_g}{\mathrm{d}\zeta^2} + (1 - Z_g)\dot{m} \,, \tag{10d}$$

where $J_j = -\frac{\partial \zeta}{\partial x_j}$. The equations for the liquid phase are:

$$\Xi_\zeta \frac{\mathrm{d}Z_l}{\mathrm{d}\zeta} = -\dot{m}\,(1 + Z_l) + \Psi\,[Z_l] \,, \tag{11a}$$

$$\Xi_\zeta \frac{\mathrm{d}m_d}{\mathrm{d}\zeta} = -\dot{m}\frac{\rho}{n_l} + \Psi\,[m_d] \,, \tag{11b}$$

$$\Xi_\zeta \frac{\mathrm{d}\,(u_{l,j}Z_l)}{\mathrm{d}\zeta} = -\dot{m}u_{l,j}(1 + Z_l) - f_j + \Psi\,[u_{l,j}Z_l] \,, \tag{11c}$$

$$\Xi_\zeta \frac{\mathrm{d}\,(Z_l h_l)}{\mathrm{d}\zeta} = -\dot{m}(1 + Z_l)h_l + \dot{m}(L - q) + \Psi\,[h_l Z_l] \,, \tag{11d}$$

where $\Psi[\phi]$ is defined as the contribution to the slip velocity due to the drag force:

$$\Psi\left[\phi\right] = \frac{\partial \zeta}{\partial x_i} \frac{\partial}{\partial \zeta} \left[\rho \phi (u_i - u_{l,i})\right] \ . \tag{12}$$

In accordance with Peters' theory for gaseous flames, the flamelet transformation assumes that the flame structure is locally one-dimensional. The formulation of an appropriate mixing-describing variable ζ is discussed in the following section.

3. Composition-space definition for counterflow spray flames

The spray flamelet equations, Eqs. (10) and (11), are derived by invoking two assumptions, namely the presence of a one-dimensional flame structure and the strict monotonicity of ζ with respect to the spatial coordinate. The last constraint is required to guarantee the existence of the derivative and that the solution remains single-valued. Identifying an appropriate definition of ζ that meets this last criterion is the central focus of this paper. Before introducing this variable, we will review previously suggested formulations from the literature.

Gaseous mixture fraction The first candidate is the classical gaseous non-normalized mixture fraction,

$$\zeta = Z_g \ , \tag{13}$$

which is defined in Eq. (2) and the corresponding conservation equation is given by Eq. (1d). This definition was used previously to parameterize the spray-flamelet equations [27]. As discussed in [27, 28, 41], the presence of a source term results in a non-conserved quantity for counterflow spray flames[1]. Furthermore, due to competing effects between evaporation and mixing, Z_g becomes non-monotonic, resulting in the multi-valued representation of the flame structure in Z_g-space. While this prevents the direct solution of the spray flamelet equations in composition space, Z_g has been used for the parameterization of spray flames using two different approaches:

- Separating the spray zone and the purely gaseous zone to identify two distinct regions where Z_g is monotonic as done in [8]. However, it will be shown in the subsequent section that this approach does not always guarantee monotonicity in these phase-separated regions when diffusion and evaporation are not spatially separated.
- Separating the flame structure at the tangent point $\mathrm{d}_x Z_g = 0$ [27]. Although this method provides a valid representation of the flame structure, the location of this inflection point is not know *a priori* and can therefore not be used in a straightforward manner as a separation indicator.

Total mixture fraction An alternative to using Z_g as describing composition variable is to also consider the contribution from the two-phase region in the definition of ζ. A possible definition of such a quantity was first proposed in [31], and further

[1]Since the definition of mixture fraction is reserved for a conserved quantity, Z_g from Eq. (1d) does not strictly represent a mixture fraction. However, for consistency reasons with previous works, we follow this convention.

investigated in [28, 41] as:

$$\zeta = Z_t = Z_g + Z_l \ . \tag{14}$$

This definition can be considered as an extension of Eq. (2). In this context it is noted that the consistency of this formulation is guaranteed by the fact that $Z_g \equiv Y_F$ for pure fuel. The conservation equation in physical space is given by [28, 41]:

$$\rho u_i \frac{\partial Z_t}{\partial x_i} = \frac{\partial}{\partial x_i}\left(\rho D \frac{\partial Z_g}{\partial x_i} + \rho(u_i - u_{l,i}) Z_l\right) - Z_t \dot{m} \ . \tag{15}$$

The evaporation source term in this equation is negative, leading to a decreasing Z_t along the material derivative. Consequently, this term will not affect the monotonicity. However, due to the differential diffusion between liquid and gaseous phase and the presence of the slip velocity, the monotonicity of Z_t is not guaranteed. This issue was discussed in [28, 41] and demonstrated in [28].

Conserved mixture fraction Another definition of a mixture fraction can be obtained by eliminating the evaporation source term, which is achieved through the following definition:

$$\zeta = Z_c = \frac{Z_g + Z_l}{1 + Z_l} \ , \tag{16}$$

with corresponding conservation equation in physical space is then:

$$\rho u_i \frac{\partial Z_c}{\partial x_i} = \frac{1}{1+Z_l}\frac{\partial}{\partial x_i}\left(\rho D \frac{\partial Z_g}{\partial x_i}\right) + \frac{1 - Z_c}{1 + Z_l}\frac{\partial}{\partial x_i}\left[\rho(u_i - u_{l,i}) Z_l\right] \ . \tag{17}$$

This definition also suffers from contributions by slip velocity and differential diffusion between gaseous and liquid phase.

Effective composition variable A composition variable that is strictly monotonic for counterflow spray flames can be obtained by restricting the two-dimensional space (Z_g, Z_l) to the 1D manifold to which the solution belongs to. By doing so, one can define a composition space variable η as the metric of the 1D manifold, i.e. its tangent in the (Z_g, Z_l)-space:

$$(\mathrm{d}\zeta)^2 = (\mathrm{d}\eta)^2 = (\mathrm{d}Z_g)^2 + (\mathrm{d}Z_l)^2 \ , \tag{18}$$

from which follows:

$$\mathrm{d}\eta = \sqrt{(\mathrm{d}Z_g)^2 + (\mathrm{d}Z_l)^2} \ , \tag{19}$$

where the sign is determined subject to the local flow structure. By combining Eqs. (19) and (5a) with Eq. (1d), the transport equation for η can be written as:

$$\begin{aligned}\rho u_i \frac{\partial \eta}{\partial x_i} &= \mathrm{sgn}(u_\eta)\sqrt{\left(\rho u_i \frac{\partial Z_g}{\partial x_i}\right)^2 + \left(\rho u_i \frac{\partial Z_l}{\partial x_i}\right)^2} \\ &= \mathrm{sgn}(u_\eta)\sqrt{\left(\frac{\partial}{\partial x_i}\left(\rho D \frac{\partial Z_g}{\partial x_i}\right) + (1-Z_g)\dot{m}\right)^2 + \left(\frac{\partial[\rho(u_i - u_{l,i})Z_l]}{\partial x_i} - \dot{m}(1+Z_l)\right)^2}\,,\end{aligned} \tag{20}$$

where $u_\eta = u_i \partial_{x_i}\eta / \sqrt{(\partial_{x_j}\eta)^2}$ is the gas velocity projected along the gradient of η. Note that this definition of η reduced to the classical gaseous mixture fraction expression in the absence of a liquid phase, guaranteeing the consistency with the single-phase flamelet formulation [24]. This follows by imposing the condition:

$$\mathrm{sgn}(u_\eta) = \mathrm{sgn}\left(u_i \partial_{x_i} Z_g / \sqrt{(\partial_{x_j} Z_g)^2}\right) \quad \text{if} \quad Z_l = 0\,. \tag{21}$$

In this context, it is noted that the definition (19) of η is based on mathematical arguments and requirements of monotonicity, positivity and degeneracy. As such, it is not directly based on physical interpretation following classical mixture-fraction argumentation. However, the mathematical definition of Eq. (19) enables comparisons with measurements, and a link between η, Z_g and Z_l is provided under the assumption of separating mixing and evaporation zones (App. B).

The particular advantage of definition (19) is that it enables a direct solution of the flamelet equations in composition space. Further, with regards to application to tabulation methods, it overcomes the ambiguity that is associated with the construction of different chemistry libraries to represent gaseous and two-phase zones. It has to be noted that the evaporation process contributes twice to the evolution of η, as it acts both on Z_g and Z_l. This double contribution is necessary for cases where the evaporation process does not happen in the mixing layer. This situation occurs for instance if a premixed two-phase flame propagates towards the fuel injection, if the liquid fuel vaporized prior to injection, or if preferential concentration occurs before the mixing layer. In this context it is also noted that η contains a source term and is therefore not a conserved scalar. Moreover, η, as defined in Eq. (19), is non-normalized. However, this does not represent an issue for numerical simulations since the resulting flamelet equations are numerically well behaved. In fact, this property is strictly not necessary to correctly identify the flame-normal direction, which only requires to monotonically increase from the oxidizer side to the spray injection side (or vice versa). The maximum value of η, found for the limiting case with separated mixing and evaporation zones, as provided in App. B, could be used to normalize this quantity, when necessary.

4. Analysis of spray flame structure

This work considers a counterflow configuration, which consists of two opposed injection slots that are separated by a distance $L = 0.02$ m along the x_1-direction, see Fig. 1. On the fuel side, a mono-disperse kerosene ($C_{10}H_{20}$) spray is injected with air. On the oxidizer side, pure air is injected. Similar to the works by Dvorjetski and Greenberg [19] and Lerman and Greenberg [11], the gaseous flow field

is assumed to be described by a constant strain rate:[1] $u_1 = -ax_1$ and $u_2 = ax_2$. Compared to gaseous flames, the boundary conditions are not imposed at infinity in order to take into account the effect of evaporation on the mixing and reaction[2]. The following gaseous boundary conditions are imposed at both sides: $T^0 = 600$ K, $Y^0_{O_2} = 0.233$, $Y^0_{N_2} = 0.767$. For the liquid phase at the spray side, the liquid-to-gas mass ratio is $Z^0_l = 0.2$. In the present study, we examine effects of the droplet diameter of the injected spray, d^0, and the strain rate, a, on the flame structure. To focus on the coupling between mass transfer, mixing and reaction processes, approximations on the evaporation model, the liquid velocity and the temperature have been invoked for the numerical solutions of the spray flame equations. These assumptions and the resulting system of equations are presented in App. A. The reaction chemistry developed in [42] for kerosene/air flames is used in the following.

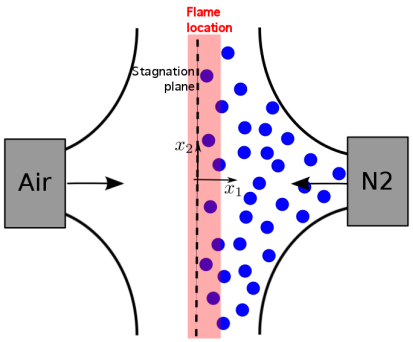

Figure 1.: Schematic of the laminar counterflow spray flame.

4.1 *Choice of composition-space variable*

The solution of the counterflow spray flame at atmospheric pressure for $d^0 = 40$ μm and $a = 100$ s^{-1} in physical space is shown in Fig. 2. The gaseous fuel from the droplet evaporation is consumed in the reaction zone, which is characterized by the high temperature region and product concentration. As a result of the fuel-rich injection condition, all oxygen that is injected at the fuel side is consumed.

The excess fuel is eventually consumed in the diffusion region, where it reacts with the oxygen that is provided from the oxidizer stream. In the following, the evaporation zone ($Z_l > 0$) identifies the spray side of the flame, and the gas side of the flame coincides with the region where $Z_l = 0$.

The different definitions for mixture fraction are evaluated and compared in Fig. 2(b). This comparison shows that gaseous (Z_g), total (Z_t) and conserved (Z_c) mixture fractions are not monotonic, which is a result of the slip velocity, the evaporation and differential diffusion effects[1] between liquid and gaseous phases. It is noted that such non-monotonic character is not due to the constant strain rate assumption, and the same effect has been observed for variable strain rate spray flames in [28].

[1] Despite the fact that this assumption is not exact for variable-density flows, it reduces the computational complexity of the counterflow while retaining the main physics. This approximation is often used as a simplified model for two-phase flame analysis.
[2] For $L \to \infty$, the pre-evaporated case is retrieved.
[1] The liquid phase does not have a diffusion term, and is therefore characterized by an infinite Lewis number.

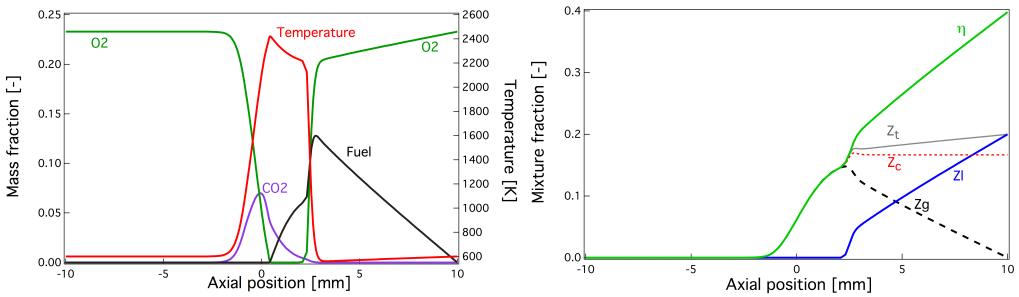

(a) Temperature and species mass fraction. (b) Gaseous, total and conserved mixture fractions.

Figure 2.: Flame structure in physical space for $d^0 = 40$ μm and $a = 100$ s^{-1}: a) temperature and species mass fraction, and b) gaseous, total and conserved mixture fractions, liquid-to-gas mass ratio and effective composition variable.

As shown in Fig. 3(a), the spray flame structure can not be easily studied in the classical mixture-fraction space. The potential of representing the spray flame structure in Z_g-space is assessed by separating the solution into two parts following two distinct approches: by distinguishing between gas and spray regions [8] or by using the maximum value of Z_g as a separation threshold [27]. However, as shown in Fig. 3(b), representing the flame structure in the Z_g-space by separating the solution into gas and spray regions is not adequate since the solution is not necessarily unique due to the non-monotonicity of Z_g in the spray region. The second strategy circumvents this issue (cfr. Fig. 3(c)), but unfortunately, the *a priori* evaluation of the maximum value of Z_g is not possible, so that this separation strategy cannot be used in a straightforward manner.

The newly proposed composition variable η addresses both issues, and the flame structure as a function of η is shown in Fig. 3(d). Compared to the mixture-fraction parameterization with respect to Z_g and Z_t, the solution is guaranteed to have a unique value for any given η. Moreover, compared to the two-zone separation, this parameterization eliminates the need for a separation criterion. The flame structure on the spray side can be correctly represented when working in physical space or in η-space.

4.2 *Flame structure in effective composition space*

The counterflow spray-flame equations (Eq. (A3)) are solved in physical space and the effective composition variable η is used to analyze the flame structure for different values of d^0 and a. The solutions for Z_g and Z_l are compared with results from an asymptotic analysis. The derivation of the analytical solution is provided in App. B, and is obtained under the assumption that evaporation and diffusion occur in two distinct regions. The analytic solutions for Z_g and Z_l present piecewise linear behaviors with respect to η when the evaporation is completed without interaction with the diffusion process. The gaseous mixture fraction reaches its maximum value $Z_g^* = Z_l^0/(1+Z_l^0) = 0.166$ at $Z_l = 0$. The spray side is then located at $\eta > Z_g^*$ and is mainly governed by evaporation. In contrast, the gas side ($\eta \leq Z_g^*$) is characterized by diffusion. By construction, η coincides with Z_g on the gas side, thereby retaining consistency with the mixture-fraction formulation for purely gaseous flames.

Results for different initial droplet diameters and strain rates are illustrated in Figs. 4 and 5, showing the solution in physical space (left) and in effective composition space (middle). The location separating the evaporation and mixing

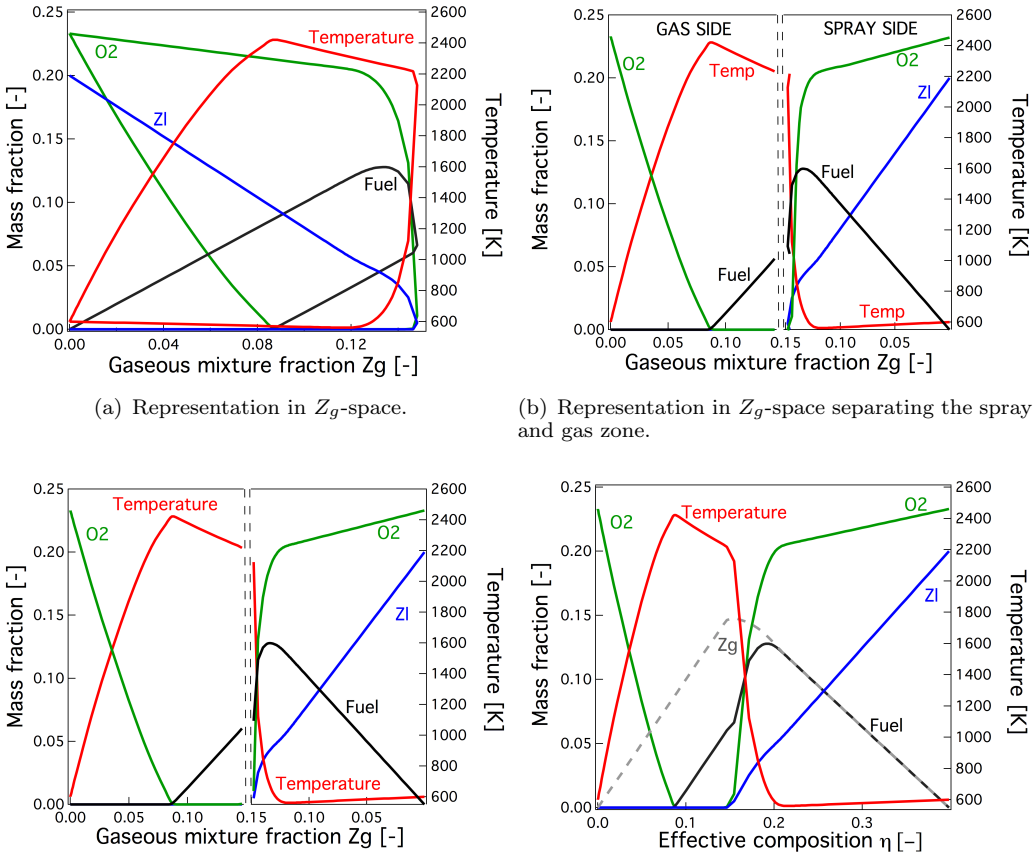

(a) Representation in Z_g-space.

(b) Representation in Z_g-space separating the spray and gas zone.

(c) Representation in Z_g-space separating the solution at maximum value of Z_g.

(d) Representation in η-space.

Figure 3.: Flame structure for $d^0 = 40$ μm and $a = 100$ s^{-1}.

regions, is indicated by the vertical blue line. To assess the significance of the diffusion process at the spray side, a budget analysis of the Z_g-transport equation (1d) is performed. In this budget analysis, the contribution of each term appearing in Eq. (1d), i.e. advection, diffusion and evaporation, is evaluated. Compared to the work of [33], the contribution of the evaporation to the budget of Z_g is not split, since both terms in Eq. (1d) relate to the sole evaporation process.

These results are presented in the right column of Figs. 4 and 5. The comparison of the results with the asymptotic solutions also allows to quantify the diffusion contribution at the spray side without looking at the budget analysis. Discrepancies with the asymptotic solutions will occur when the diffusion and evaporation zones overlap. Indeed, diffusion contributions in the spray region are apparent in Figs. 4 and 5 as deviation from the linear behavior of Z_g with respect to η on the spray side. The region where diffusion affects the results is then presented in gray in all figures based on the Z_g-profiles. The blue vertical line separates the spray side from the gas side based on the Z_l-profiles.

4.2.1 Effects of droplet diameter on spray-flame structure

Results for a constant strain rate of $a = 100$ s^{-1} and three different initial droplet diameters of $d^0 = \{20, 40, 80\}$ μm are presented in Fig. 4. For $d^0 = 20$ μm (Fig. 4(a)), the liquid fuel fully evaporates before reaching the flame reaction zone, and the high temperature region is confined to the gas region of the flame. By

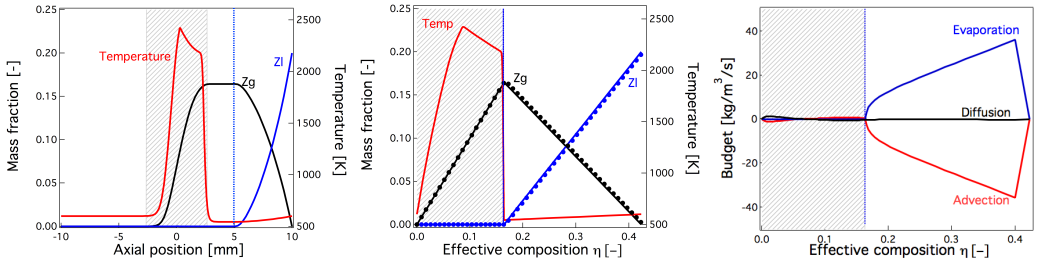

(a) Initial droplet diameter: $d^0 = 20$ μm.

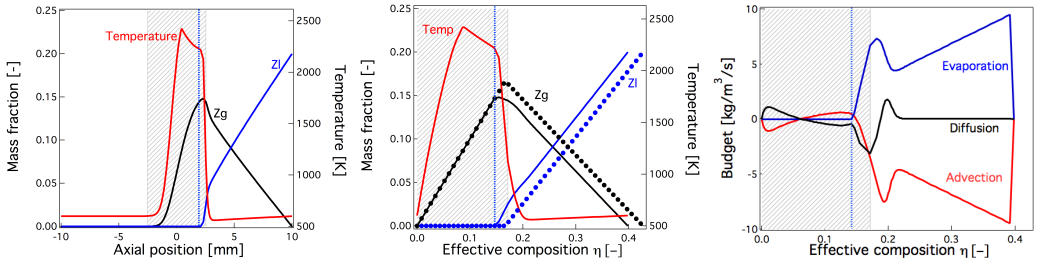

(b) Initial droplet diameter: $d^0 = 40$ μm.

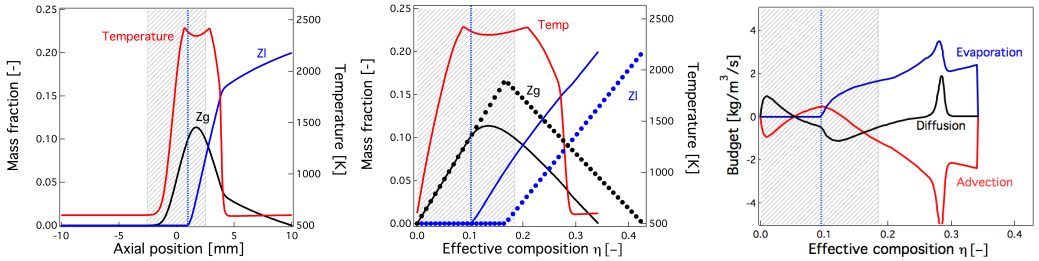

(c) Initial droplet diameter: $d^0 = 80$ μm.

Figure 4.: Flame structure obtained from the solution in physical space for $a = 100$ s^{-1} as a function of different initial droplet diameters d^0: solution in x-space (left), η-space (middle), and budget analysis (right) of Z_g-conservation equation (Eq. (1d)); the gray area corresponds to the diffusion zone; the blue vertical line separates the spray side from the gas side. For comparison, asymptotic solutions for Z_g and Z_l are shown by symbols.

considering the budget analysis, it can be seen that the diffusion contribution on the spray side is negligible for small droplet diameters. This is further confirmed by comparisons with the asymptotic solution for the gaseous mixture fraction (shown by symbols), which is in very good agreement with the simulation results.

By increasing the initial droplet diameter to $d^0 = 40$ μm, shown in Fig. 4(b), it can be seen that a small amount of liquid fuel reaches the preheat zone of the flame. The evaporation is not separated anymore from the diffusion region: as shown in the right panel of Fig. 4(b), the diffusive part of the budget can no longer be neglected close to the maximum value of Z_g. This may also be recognized by comparing the numerical results with the asymptotic profiles. Here, the maximum values for η and Z_g are small compared to the analytic solution, provided that the underlying modeling hypothesis of distinct evaporation and mixing zones is invalid.

For the case with $d^0 = 80$ μm (Fig. 4(c)) liquid fuel is penetrating into the reaction zone, and a high temperature region and a second heat-release region on the spray side can be observed. This complex flame structure is clearly visible in the η-space. Moreover, as evidenced by the overlap between the gray region and

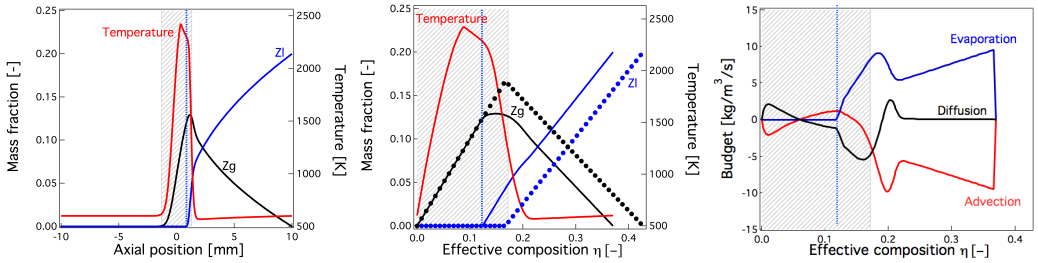

(a) Strain rate: $a = 200\ \mathrm{s}^{-1}$.

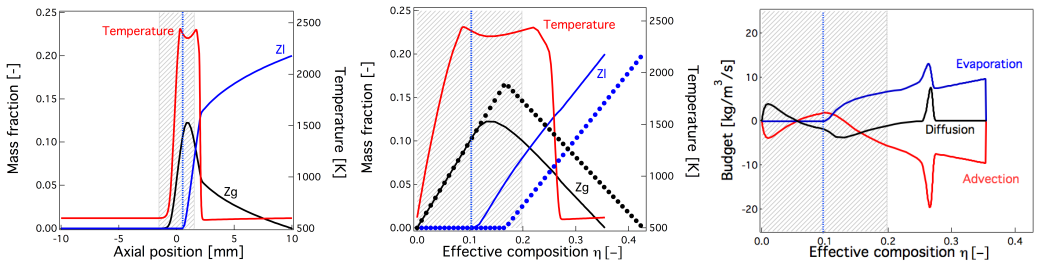

(b) Strain rate: $a = 400\ \mathrm{s}^{-1}$.

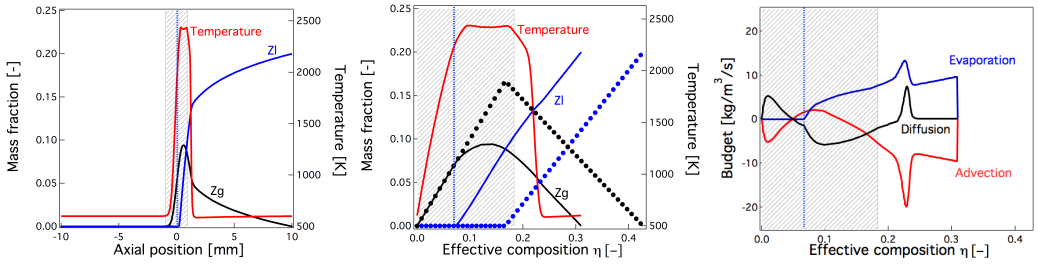

(c) Strain rate: $a = 600\ \mathrm{s}^{-1}$.

Figure 5.: Flame structure obtained from the solution in physical space for $d^0 = 40\ \mu$m as a function of different strain rates: solution in x-space (left), η-space (middle), and budget analysis (right) of Z_g-conservation equation (Eq. (1d)); the gray area corresponds to the diffusion zone; the blue vertical line separates the spray side from the gas side. For comparison, asymptotic solutions for Z_g and Z_l are shown by symbols.

the liquid volume fraction Z_l, as well as by the budget analysis, both diffusive and evaporative contributions are mixed. These interaction processes are not represented by the asymptotic solution, which relies on the spatial separation between both processes.

Considering the η-space, the effect of the droplet diameter on the flame structure is clearly identified. For all three cases considered, the first temperature peak is located on the gas side at stoichiometric condition. However, with increasing initial droplet diameter, a second temperature peak is formed on the spray side, which identifies the transition from a single-reaction to a double-reaction flame structure for large droplets, as observed in [16, 23]. Moreover, by comparing profiles of Z_g and Z_l with the analytic solution, the diffusive contribution on the spray side can be clearly recognized. By increasing the droplet diameter, diffusion effects become increasingly important in the spray region, and the diffusive processes overlap with evaporation. These effects are not reproduced by the analytic solution that is derived in App. B.

4.2.2 Effects of strain rate on spray-flame structure

Results for different strain rates $a = \{200, 400, 600\}$ s^{-1} and fixed initial droplet diameter of $d^0 = 40$ μm are presented in Fig. 5. Compared to the results in physical space for a strain rate of $a = 100$ s^{-1} (Fig. 4(b)), the flame structure in Fig. 5(a) is confined to a narrow region for $a = 200$ s^{-1}. However, the representation of the flame structure with respect to the effective composition variable η provides a clear description of the different regions that are associated with heat release and diffusion. The comparison with the analytic profiles provides an assessment of competing effects between diffusion, advection, and evaporation.

The flame structure for a strain rate of $a = 400$ s^{-1} is shown in Fig. 5(b). For this condition, a double-flame structure is observed in which the primary heat-release zone is formed on the spray side and the unburned vaporized fuel is consumed in a secondary reaction zone on the gaseous side of the flame. This result is similar to that presented in [28], but has the opposite behavior compared to the findings of [33], for which a double-flame structure is observed for low strain rates. Since, however, this study used methanol or ethanol, for which the latent heat is twice larger than that of kerosene used here and in [28], there is no contradiction between the three studies. The different reaction zones are conveniently identified in composition space, and the budget analysis provides a clear description of the contributions arising from a balance between diffusion and advection in the absence of evaporation effects.

By further increasing the strain rate to a value of $a = 600$ s^{-1} a high-temperature region is observed on the spray side (Fig. 5(c)). However, compared to the case with $a = 400$ s^{-1} the two heat-release zones are closer without exhibiting a significant reduction in temperature. At this condition, the flame on the gas side is highly strained, leading to a reduction of the maximum temperature (from 2400 to 2000 K) and both temperature peaks are located on the spray side. In comparison, the maximum temperature on the spray side is less affected by variations in strain rate.

5. Derivation of spray flamelet equations in effective composition space

One of the main motivations for introducing the monotonic composition-space variable η is to enable the direct solution of Eqs. (10) and (11) in composition space.

Rewriting Eq. (8) by introducing the effective composition space variable η and the transformation operators (7), the term Ξ_η (corresponding to the advection term in Eq. (20)) can be written as:

$$\Xi_\eta = \mathrm{sgn}(u_\eta)\sqrt{\left(\rho u_i \frac{\partial Z_g}{\partial x_i}\right)^2 + \left(\rho u_i \frac{\partial Z_l}{\partial x_i}\right)^2}, \tag{22}$$

$$= \mathrm{sgn}(u_\eta)\left\{\left(\frac{\mathrm{d}Z_g}{\mathrm{d}\eta}\left[\frac{\rho D}{2}\frac{\mathrm{d}}{\mathrm{d}\eta}\left(\frac{\chi_\eta}{2D}\right) + \frac{\chi_\eta}{2D}\frac{\mathrm{d}(\rho D)}{\mathrm{d}\eta}\right] + \frac{\rho\chi_\eta}{2}\frac{\mathrm{d}^2 Z_g}{\mathrm{d}\eta^2} + (1-Z_g)\dot{m}\right)^2 + \left(\sqrt{\frac{\chi_\eta}{2D}}\frac{\mathrm{d}[\rho Z_l(u_i - u_{l,i})]}{\mathrm{d}\eta} - \dot{m}\,(1+Z_l)\right)^2\right\}^{1/2}. \tag{23}$$

By assuming a constant pressure along the η-direction, we obtain the complete

spray-flamelet equations:

$$\Xi_\eta^* \frac{\mathrm{d}u_j}{\mathrm{d}\eta} = \frac{\mu}{D}\frac{\chi_\eta}{2}\frac{\mathrm{d}^2 u_j}{\mathrm{d}\eta^2} + (u_j - u_{l,j})\dot{m} - f_j \ , \tag{24a}$$

$$\Xi_\eta^\dagger \frac{\mathrm{d}Y_k}{\mathrm{d}\eta} = \frac{\rho\chi_\eta}{2}\frac{\mathrm{d}^2 Y_k}{\mathrm{d}\eta^2} + (\delta_{kF} - Y_k)\dot{m} + \dot{\omega}_k \ , \tag{24b}$$

$$\Xi_\eta^\dagger \frac{\mathrm{d}T}{\mathrm{d}\eta} = \frac{\rho\chi_\eta}{2}\frac{\mathrm{d}^2 T}{\mathrm{d}\eta^2} + \dot{m}\left(T_l - T - \frac{q}{c_p}\right) + \dot{\omega}_T \ , \tag{24c}$$

$$\Xi_\eta^\dagger \frac{\mathrm{d}Z_g}{\mathrm{d}\eta} = \frac{\rho\chi_\eta}{2}\frac{\mathrm{d}^2 Z_g}{\mathrm{d}\eta^2} + (1 - Z_g)\dot{m} \ , \tag{24d}$$

$$\Xi_\eta \frac{\mathrm{d}Z_l}{\mathrm{d}\eta} = -\dot{m}\,(1 + Z_l) + \Psi\left[Z_l\right] \ , \tag{24e}$$

$$\Xi_\eta \frac{\mathrm{d}m_d}{\mathrm{d}\eta} = -\dot{m}\frac{\rho}{n_l} + \Psi\left[m_d\right] \ , \tag{24f}$$

$$\Xi_\eta \frac{\mathrm{d}(u_{l,j}Z_l)}{\mathrm{d}\eta} = -f_j - \dot{m}u_{l,j}(1 + Z_l) + \Psi\left[u_{l,j}Z_l\right] \ , \tag{24g}$$

$$\Xi_\eta \frac{\mathrm{d}(Z_l h_l)}{\mathrm{d}\eta} = -\dot{m}h_l(1 + Z_l) + \dot{m}(L_v - q) + \Psi\left[h_l Z_l\right] \ , \tag{24h}$$

where the following quantities are introduced:

$$\Xi_\eta^* = \Xi_\eta - \left[\frac{\mu}{2}\frac{\mathrm{d}}{\mathrm{d}\eta}\left(\frac{\chi_\eta}{2D}\right) + \frac{\chi_\eta}{2D}\frac{\mathrm{d}\mu}{\mathrm{d}\eta}\right] \ , \tag{25a}$$

$$\Xi_\eta^\dagger = \Xi_\eta - \left[\frac{\rho D}{2}\frac{\mathrm{d}}{\mathrm{d}\eta}\left(\frac{\chi_\eta}{2D}\right) + \frac{\chi_\eta}{2D}\frac{\mathrm{d}(\rho D)}{\mathrm{d}\eta}\right] \ , \tag{25b}$$

$$\Psi\left[\phi\right] = \frac{\partial\eta}{\partial x_i}\frac{\partial}{\partial\eta}\left[\rho\phi(u_i - u_{l,i})\right] \ , \tag{25c}$$

$$\chi_\eta = 2D\left(\frac{\partial\eta}{\partial x_i}\right)^2 . \tag{25d}$$

To confirm consistency, it can be seen that the spray-flamelet formulation (24) reduces to the classical gaseous mixture-fraction formulation in the absence of a liquid phase. Moreover, its consistency is guaranteed by construction, since no assumption has been applied to rewrite the general equation system, Eqs. (10) and (11), into the formulation (24), except for $d_\eta p = 0$.

To solve Eqs. (24) in the effective composition space, closure models are required for the terms $\partial_{x_i}\eta$ and $(\partial_{x_i}\eta)^2$ that appear in the expressions for the slip velocity and the scalar dissipation rate (Eqs. (25c) and (25d)). Before discussing in Sec. 5.2 the validity of the closure models developed in Apps. C and D, we will first verify the feasibility of directly solving Eqs. (24) in composition space through direct comparisons with spray-flame solutions from physical space. For this, the spray-flamelet equations (24) are solved using expressions for χ_η and Ψ that are directly extracted from the physical-space spray-flame solutions. In the following, the assumptions described in App. A will be used to simplify the numerical simulations. However, it is noted that the spray flamelet equations (24) are general and do not rely on such assumptions.

5.1 *Feasibility of η-space simulations*

A spray-flamelet formulation has been proposed in Z_g-composition space by [27]. However, due to the non-monotonicity of Z_g, the system could not be directly solved in composition space. Instead, the system was solved in physical space and contributions of each term from the solution of the counterflow spray flame was post-processed in the Z_g-space.

In contrast, the introduction of η enables the direct solution of the spray-flamelet equations in composition space. To demonstrate the consistency of the spray-flamelet formulation, one-dimensional counterflow spray flames are solved in η-space by invoking the assumptions that were introduced in App. A.

A direct comparison of the solutions obtained in physical space using 400 mesh points with adaptive refinement (solid lines) and in composition space with 100 mesh points with equidistant grid spacing (symbols) are shown in Fig. 6. The operating conditions correspond to the case discussed in Sec. 4 ($d_0 = 40$ μm and $a = 100$ s^{-1}). The excellent agreement between both solutions confirms the validity of the newly proposed spray-flamelet formulation for providing a viable method for the flame-structure representation and as method for solving the spray-flamelet equations in composition space.

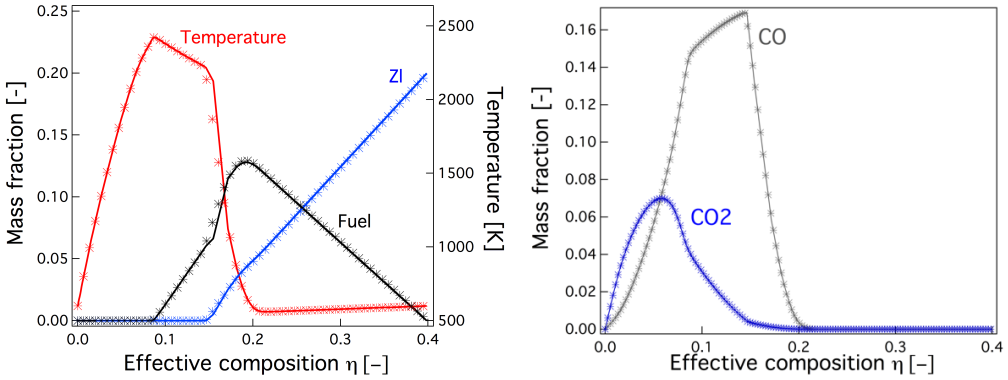

(a) Temperature, fuel and liquid-to-gas mass fractions.

(b) Mass fractions of CO_2 and CO.

Figure 6.: Comparison of spray-flame structure for $d^0 = 40$ μm and $a = 100$ s^{-1} obtained from the solution in physical space (symbols) and in η-composition space (solid lines). To facilitate a direct comparison, χ_η is extracted from the x-space solution.

5.2 *Closure models for χ_η and Ψ*

In this section, the performance of the closure model for the scalar dissipation rate χ_η ~~on the simulation results~~ is assessed. Here, we consider the formulation of χ_η developed in App. C. This closure model is based on the linearization of the evaporation model, controlled by the constant vaporization time τ_v, and the spatial separation of evaporation and diffusion. A model for the slip-velocity term Ψ, under consideration of the small Stokes-number limit based on the drag Stokes number $\mathrm{St}_d = a\tau_d$, is also provided in App. D. Since the numerical simulation considers the limiting case of zero slip velocity, the only unclosed term is the scalar dissipation rate χ_η. This term is essential not only to characterize the gas side of the flame structure, but also to account for effects of advection, mixing, and evaporation

on the liquid spray side. To ensure consistency with the assumptions that were introduced in developing the closure for χ_η in App. C, we utilize the linearized evaporation model, which introduces a constant evaporation time τ_v (see Eq. (B2) in App. B). The solution of the spray-flame equations in physical space is then compared against the solution obtained by solving the spray-flamelet equations in η-space, for which χ_η is either directly extracted from the solution in physical space or from the analytical expression given by Eq. (C5). Two cases are considered here: $\tau_v = 0.005$ s and $\tau_v = 0.02$ s. Comparing the flame structure with results obtained in physical space for the evaporation model of Sec. 4, these cases are representative for conditions of $d^0 = 20$ μm and $d^0 = 60$ μm, respectively.

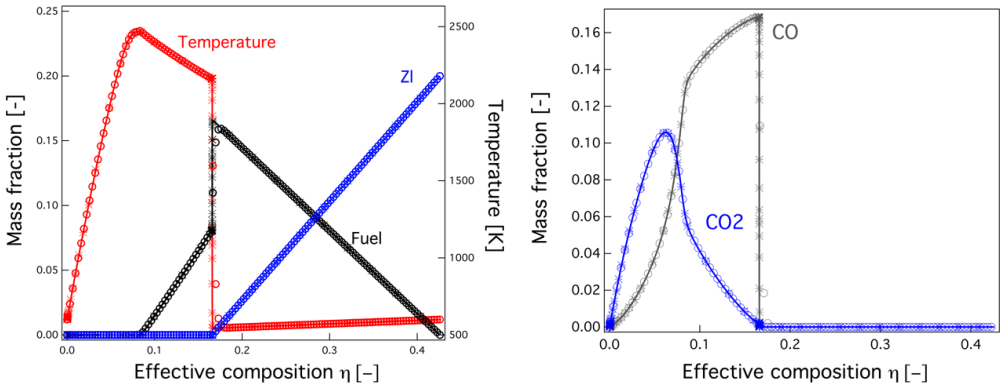

(a) Temperature, fuel and liquid-to-gas mass fractions.

(b) Mass fractions of CO_2 and CO.

Figure 7.: Comparison of spray-flame solution in η-space using the linearized evaporation model for $\tau_v = 0.005$ s. The solution obtained in physical space is projected onto the η-space (solid lines), spray-flamelet solution in η-space with χ_η extracted from x-space solution (stars) and from analytic closure model (open circles). The strain rate is $a = 100$ s^{-1}.

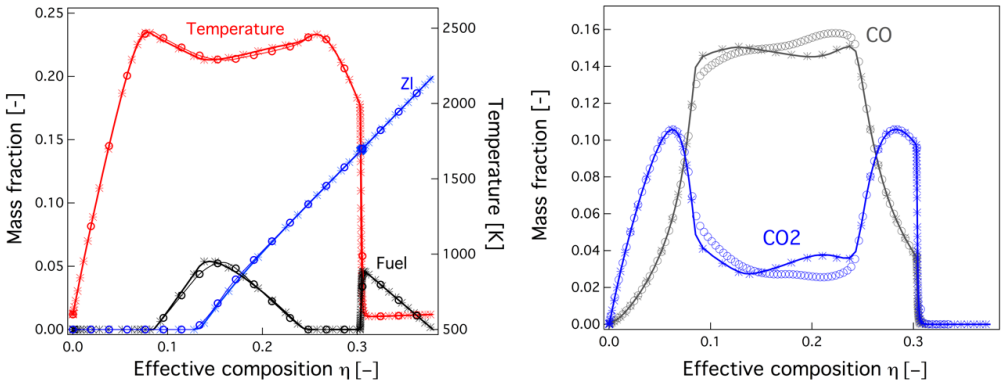

(a) Temperature, fuel and liquid-to-gas mass fractions.

(b) Mass fractions of CO_2 and CO.

Figure 8.: Comparison of spray-flame solution in η-space using the linearized evaporation model for $\tau_v = 0.02$ s. The solution obtained in physical space is projected onto the η-space (solid lines), spray-flamelet solution in η-space with χ_η extracted from x-space solution (stars) and from analytic closure model (open circles). The strain rate is $a = 100$ s^{-1}.

The comparison of the flame structures for $\tau_v = 0.005$ s is presented in Fig. 7. The maximum value of η is slightly overestimated when using the analytical expression for χ_η, resulting in a small shift of the flame-structure profile in effective composition space. This can be attributed to the fact that evaporation and diffusion overlap in a small region. However all solutions give comparable results, confirming the validity of the model for small Stokes numbers.

The flame structure for $\tau_v = 0.02$ s is analyzed in Fig. 8. The flame structure is substantially different from the other case, showing the presence of a double-flame and an overlap of the evaporation and diffusion regions. The results in effective composition space are in good agreement with the physical-space solution, but some differences can be seen in the region where evaporation and diffusion overlap. Radicals and intermediate species are expected to be more sensitive to strain rate and, consequently, to be more sensitive to the closure model for χ_η. This can be observed by comparing the CO mass fraction in Figs. 7(b) and 8(b). For $\tau_v = 0.005$ s, the assumptions underlying the χ_η closure model are verified, leading to a good agreement between the physical results and the two composition-space solutions. In contrast, for $\tau_v = 0.02$ s diffusion and evaporation overlap, violating the assumptions that we invoked in the development of the closure for χ_η. Indeed, some discrepancies for the CO-profile are noted for the calculation with the analytical closure model, whereas the calculation using χ_η extracted from the x-space solution is still in good agreement with the physical space solution. Nevertheless, the overall agreement remains satisfactory for all simulations.

The same analysis was performed using the d^2-evaporation model of App. A (Eq. (A1)) and variable density. Results show the same trend discussed for constant τ_v, and this will be further examined in the following section. Although further improvements for the closure model of χ_η are desirable to extend its applicability to larger values of τ_v, results obtained from the η-space solution are in satisfactory agreement with the x-space solutions.

5.3 *Effect of droplet diameter and strain rate: bifurcation and hysteresis*

Effects of droplet diameter and strain rate on the flame structure are examined by solving the spray flamelet equations (Eqs. (A6)) in η-space using the analytical closure for χ_η and the d^2-evaporation model that we introduced in App. A[1]. Starting from the solution for $d^0 = 10$ μm and $a = 100$ s^{-1}, the droplet diameter at injection is successively increased until $d^0 = 80$ μm at an increment of 10 μm.

Results for $d^0 = \{20, 40, 80\}$ μm are presented in Fig. 9. It can be seen that for small droplet diameters a single-reaction structure is observed whereas for larger droplet diameters ($d^0 > 50$ μm) the flame is characterized by a double-reaction structure. Starting from the solution for $d^0 = 80$ μm, the droplet diameter at injection is incrementally decreased until $d^0 = 10$ μm. The double-reaction structure is retained until $d^0 = 40$ μm with a transition from double- to single-reaction structure occurring at $d^0 = 30$ μm. Hence, for a droplet diameter between $d^0 = 40$ μm and $d^0 = 60$ μm, depending on the initial condition two different flame structures are found. This is shown for the case of $d^0 = 40$ μm in Fig. 9(b), obtained when increasing the droplet diameter, and in Fig. 9(d), corresponding to the transition from double- to single-reaction structure. The occurrence of this bifurcation was suggested by Continillo and Sirignano [7] and confirmed by Gutheil [16], and is

[1]To take into account the variability of the evaporation time, the vaporization Stokes number is approximated by $\mathrm{St}_v = a\tau_{v,\mathrm{ref}} \left(d/d_{\mathrm{ref}}\right)^2$ where $\tau_{v,\mathrm{ref}} = 0.04$ s and $d_{\mathrm{ref}} = 40$ μm.

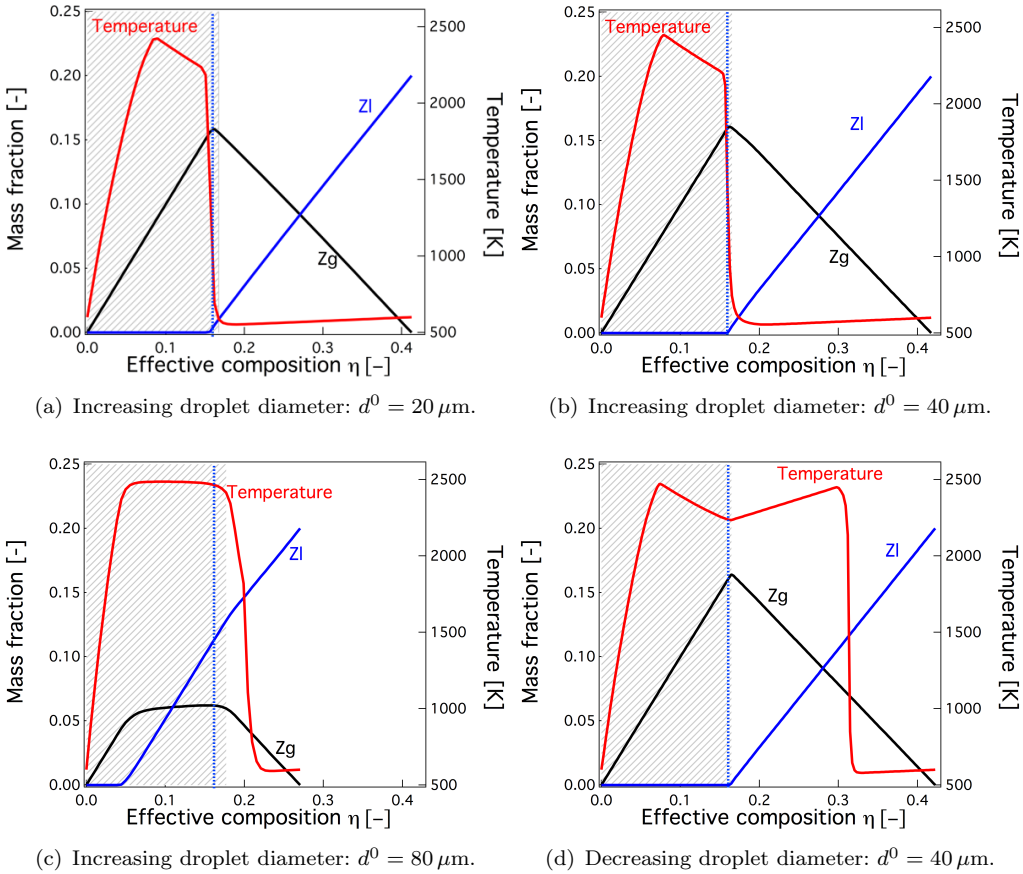

(a) Increasing droplet diameter: $d^0 = 20\,\mu$m.

(b) Increasing droplet diameter: $d^0 = 40\,\mu$m.

(c) Increasing droplet diameter: $d^0 = 80\,\mu$m.

(d) Decreasing droplet diameter: $d^0 = 40\,\mu$m.

Figure 9.: Counterflow flame structure in η-space for a) $d^0 = 20\,\mu$m, b) $d^0 = 40\,\mu$m for increasing droplet diameter, and c) $d^0 = 80\,\mu$m and d) $d^0 = 40\,\mu$m for decreasing droplet diameter. Spray-flamelet equations are solved in η-space using the analytic closure for χ_η developed in App. C (symbols). The gray area corresponds to the diffusion zone; the blue vertical line separates the spray side from the gas side.

attributed to the increased nonlinearity that is introduced through the evaporation term. Capturing this phenomenon is a confirmation of the suitability of our flamelet formulation for the description of the physics of spray flames.

The behavior of the flame to a variation in the droplet diameter strongly depends on the evaporation model and the reaction chemistry. Vié et al. [23] identified a hysteresis for droplet diameter variations, which was characterized by a double-branch structure. Following this analysis, the mean flamelet temperature is used as a robust metric to distinguish between single- and double-reaction structures:

$$\overline{T} = \frac{1}{\max(\eta)} \int_0^{\max(\eta)} T(\eta)\,\mathrm{d}\eta\,. \tag{26}$$

In the following, the mean flame temperature is normalized by the corresponding value for $d^0 = 10\ \mu$m and $a = 100\ \mathrm{s}^{-1}$. Results for variations in droplet diameter are shown in Fig. 10 to represent the hysteresis loop. Results from the physical space are also included in Fig. 10 for comparison. The hysteresis behavior is captured by both formulations, and slightly higher values for the double-reaction structure are obtained from the solution in physical space.

The effect of the strain rate is further investigated. Starting from the solution

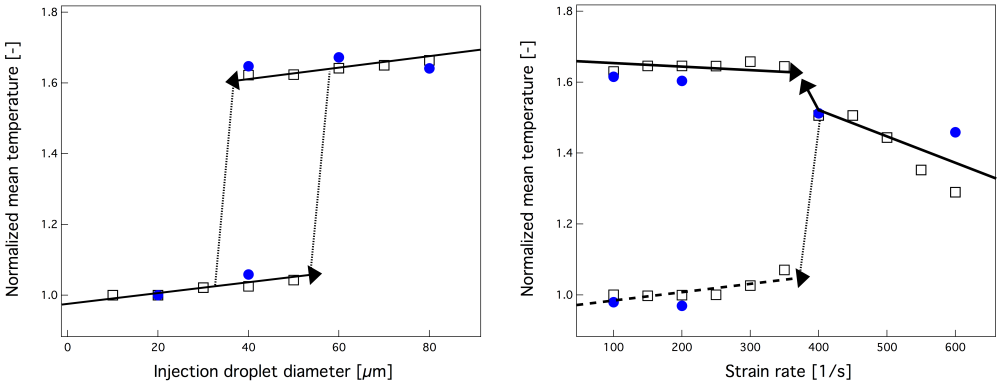

(a) Variations in droplet diameter. (b) Variations in strain rate.

Figure 10.: Counterflow solution in η-space for a) variations in droplet diameter at a fixed strain rate of $a = 100$ s^{-1} and b) variations in strain rate for a fixed droplet diameter of $d^0 = 40$ μm. Solution from η-space formulation is shown by open squares and corresponding reference solution in physical space is shown by blue closed circles. Arrows indicate the direction of the parametric variation.

for $d^0 = 40$ μm and $a = 100$ s^{-1} at the lower branch in Fig. 10(a). The strain rate is initially increased in increments of $\Delta a = 50$ s^{-1} until $a = 600$ s^{-1}. Results for $a = \{200, 400, 600\}$ s^{-1} are illustrated in Fig. 11. These results reproduce the

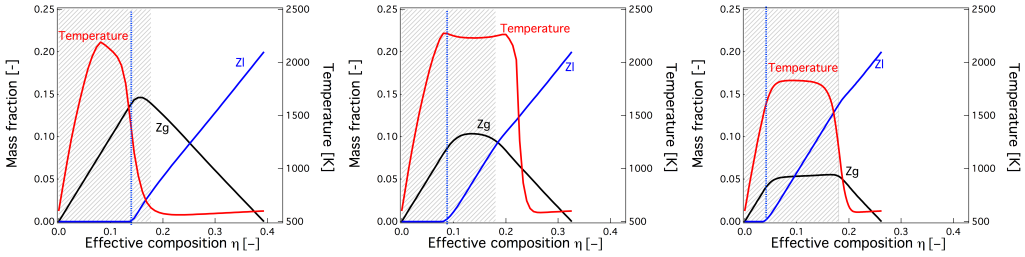

(a) $a = 200$ s^{-1}. (b) $a = 400$ s^{-1}. (c) $a = 600$ s^{-1}.

Figure 11.: Counterflow flame structure in η-space for $d^0 = 40$ μm and increasing strain rates of a) $a = 200$ s^{-1}, b) 400 s^{-1} and c) 600 s^{-1}. Solution obtained in η-space using the closure for χ_η developed in App. C. The gray area corresponds to the diffusion zone; the blue vertical line separates the spray side from the gas side.

behavior of the x-space solution from Sec. 4, with a transition from a single- to a double-reaction structure at $a = 350$ s^{-1}. However, when starting from a double-reaction solution for $a > 350$ s^{-1} and decreasing the strain rate, the flame retains its double-reaction structure. Moreover, it has been verified that when starting from the double-reaction solution for $d^0 = 40$ μm and $a = 100$ s^{-1}, the double-reaction structure is retrieved both by increasing and by decreasing the droplet diameter. Consequently, a stable branch is identified for which the flame structure is of double-reaction type, whereas the solution stays on the lower single-reaction structure branch of Fig. 10(b) as long as the strain rate remains below 350 s^{-1}. This type of bifurcation was also observed in [23], where two branches were identified without the occurrence of an hysteresis[1]. It may also be noted that the temperature

[1]It is noted that the flame transition from single- to double-reaction and *vice versa* is sensitive to the

is overestimated for the highest values of the strain rate when solving the system in η-space. This is due to the fact that the assumptions underlying the closure for χ_η are not valid for high strain rate values, as discussed in Sec. 4.2. However, the proposed closure for χ_η is a first attempt to model the scalar dissipation rate of spray flame. With its shortcomings, the proposed η-space formulation is able to reproduce effects of droplet diameter and strain rate on the spray flame structure. This capability of the spray-flamelet formulation was further demonstrated by showing that it captures the hysteresis process.

6. Conclusions

An effective composition variable η was proposed to study the structure of spray flames in composition space in analogy with the classical theory for purely gaseous diffusion flames. Unlike previous attempts [27, 32] that have been used to describe a mixture-fraction variable, the newly proposed effective composition variable is monotonic, thereby enabling the solution of spray flame in composition space. Furthermore, since this new definition is also based on the liquid-to-gas mass ratio, it can capture the evolution of the disperse phase even if no evaporation occurs, which is not the case for purely gaseous-based definitions.

This new composition space was used to analyze counterflow spray flames that were simulated in physical space, showing its ability to represent the spray-flame structure. Subsequently, a flamelet formulation was derived and solved, showing the practical feasibility of directly evaluating the resulting spray flamelet equations in η-space. From these flamelet equations arises the necessity of closures for the scalar dissipation rate and the slip velocity. A simplified model was proposed and the potential of the closure for χ_η was verified against solutions in physical space. The complete flamelet formulation is used to investigate effects of strain rate and droplet diameter on the flame behavior, reproducing the bifurcation and hysteresis of the flame structure.

The proposed spray flamelet formulation represents a theoretical tool for the asymptotic analysis of spray flames [11] in composition space. Formulation in an Eulerian form can be extended to polydisperse flow fields, by using for instance a multifluid formulation [43] for the droplet phase. This enables the consideration of the liquid mixture fraction as the sum of all liquid size volume fractions, where the polydispersity only acts on the overall vaporization rate. Another interesting extension could be to take into account large Stokes-number effect such as droplet velocity reversal [6], which can be done by introducing additional droplet classes and adding each droplet class contribution to the mixture fraction definition. This work is also a first step towards the development of spray-flamelet based turbulent models, which will require development of subgrid scales model for the composition space variable η as well as evaporation source terms.

Acknowledgments

The authors gratefully acknowledge financial support through NASA with Award Nos. NNX14CM43P and NNM13AA11G and from SAFRAN. Helpful discussions with Prof. Sirignano on the spray-flamelet formulation are appreciated.

numerical procedure that is used to vary the strain rate and droplet diameter.

Disclosure statement

Conflict of interest: The authors declare that they have no conflict of interests.
Research involving Human Participants and/or Animals: Not applicable for this paper.
Informed consent: All the authors approve this submission.

References

[1] G.M. Faeth, *Evaporation and combustion of sprays*, Prog. Energy Comb. Sci. 9 (1983), pp. 1–76.
[2] R. Borghi, *Background on droplets and sprays*, in *Combustion and Turbulence in Two Phase Flows, Lecture Series 1996-02*, Von Karman Institute for Fluid Dynamics, 1996.
[3] W.A. Sirignano, *Fluid dynamics and transport of droplets and sprays,* 2^{nd} *edition*, Cambridge University Press, 2010.
[4] P. Jenny, D. Roekaerts, and N. Beishuizen, *Modeling of turbulent dilute spray combustion*, Prog. Energy Comb. Sci. 38 (2012), pp. 846–887.
[5] W.A. Sirignano, *Advances in droplet array combustion theory and modeling*, Prog. Energy Comb. Sci. 42 (2014), pp. 54–86.
[6] A.L. Sanchez, J. Urzay, and A. Liñán, *The role of separation of scales in the description of spray combustion*, Proc. Combust. Inst. 35 (2014), pp. 1549–1577.
[7] G. Continillo and W.A. Sirignano, *Counterflow spray combustion modeling*, Combust. Flame 81 (1990), pp. 325–340.
[8] C. Hollmann and E. Gutheil, *Diffusion flames based on a laminar spray flame library*, Combust. Sci. Tech. 135 (1998), pp. 175–192.
[9] S. Russo and A. Gomez, *The extinction behavior of small interacting droplets in cross-flow*, Combust. Flame 130 (2002), pp. 215–224.
[10] S. Russo and A. Gomez, *Physical characterization of laminar spray flames in the pressure range 0.1–0.9 MPa*, Combust. Flame 145 (2006), pp. 339–356.
[11] S. Lerman and J.B. Greenberg, *Spray diffusion flames - an asymptotic theory*, Atomization and Sprays 20 (2010), pp. 1047–1064.
[12] S.C. Li, P.A. Libby, and F.A. Williams, *Experimental and theoretical studies of counterflow spray diffusion flames.*, in *24th Symp. (Int.) on Combustion*, The Combustion Institute, Pittsburgh, 1992, pp. 1503–1512.
[13] N. Darabiha, F. Lacas, J.C. Rolon, and S. Candel, *Laminar counterflow spray diffusion flames: A comparison between experimental results and complex chemistry calculations*, Combust. Flame 95 (1993), pp. 261–275.
[14] M. Massot, M. Kumar, M.D. Smooke, and A. Gomez, *Spray counterflow diffusion flames of heptane: Experiments and computations with detailed kinetics and transport*, Proc. Combust. Inst. 27 (1998), pp. 1975–1983.
[15] E. Gutheil and W.A. Sirignano, *Counterflow spray combustion modeling with detailed transport and detailed chemistry*, Combust. Flame 113 (1998), pp. 92–105.
[16] E. Gutheil, *Multiple solutions for structures of laminar counterflow spray flames*, Prog. Comput. Fluid Dyn. 5 (2005), pp. 414–419.
[17] H. Watanabe, R. Kurose, S.M. Hwang, and F. Akamatsu, *Characteristics of flamelets in spray flames formed in a laminar counterflow*, Combust. Flame 148 (2007), pp. 234–248.
[18] J.B. Greenberg and N. Sarig, *Coupled evaporation and transport effects in counterflow spray diffusion flames*, Combust. Sci. Tech. 92 (1993), pp. 1–33.
[19] A. Dvorjetski and J.B. Greenberg, *Steady-state and extinction analyses of counterflow spray diffusion flames with arbitrary finite evaporation rate*, Combust. Sci. Tech. 174 (2002), pp. 187–208.
[20] A. Dvorjetski and J.B. Greenberg, *Analysis of steady state polydisperse counterflow spray diffusion flames in the large Stokes number limit*, Proc. Combust. Inst. 32 (2009), pp. 2205–2214.
[21] V.S. Santoro, D.C. Kyritsis, and A. Gomez, *An experimental study of vortex-flame interaction in counterflow spray diffusion flames*, Proc. Combust. Inst. 28 (2000), pp. 1023–1030.
[22] V.S. Santoro and A. Gomez, *Extinction and reignition in counterflow spray diffusion flames interacting with laminar vortices*, Proc. Combust. Inst. 29 (2002), pp. 585–592.

[23] A. Vié, B. Franzelli, Y. Gao, T. Lu, H. Wang, and M. Ihme, *Analysis of segregation and bifurcation in turbulent spray flames: a 3d counterflow configuration*, Proc. Combust. Inst. 35 (2014), pp. 1675–1683.

[24] N. Peters, *Laminar diffusion flamelet models in non-premixed turbulent combustion*, Prog. Energy Comb. Sci. 10 (1984), pp. 319–339.

[25] R. Borghi, *The links between turbulent combustion and spray combustion and their modelling*, in *8th International Symposium on Transport Phenomena in Combustion*, 1996, pp. 1–18.

[26] F. Demoulin and R. Borghi, *Assumed pdf modeling of turbulent spray combustion*, Combust. Sci. Tech. 158 (2000), pp. 249–271.

[27] H. Olguin and E. Gutheil, *Influence of evaporation on spray flamelet structures*, Combust. Flame 161 (2014), pp. 987–996.

[28] A. Vié, B. Franzelli, B. Fiorina, N. Darabiha, and M. Ihme, *On the description of spray flame structure in the mixture fraction space*, Annual Research Briefs, Center for Turbulence Research, Stanford (2013), pp. 93–106.

[29] W.A. Sirignano, *A general superscalar for the combustion of liquid fuels*, Proc. Combust. Inst. 29 (2002), pp. 535–542.

[30] R.W. Bilger, *A mixture fraction framework for the theory and modeling of droplets and sprays*, Combust. Flame 158 (2011), pp. 191–202.

[31] N.S.A. Smith, C.M. Cha, H. Pitsch, and J.C. Oefelein, *Simulation and modeling of the behavior of conditional scalar moments in turbulent spray combustion*, Proceedings of the Summer Program 2000, Center for Turbulence Research, Stanford University (2000), pp. 207–218.

[32] K. Luo, F. Jianren, and K. Cen, *New spray flamelet equations considering evaporation effects in the mixture fraction space*, Fuel 103 (2014), pp. 1154–1157.

[33] H. Olguin and E. Gutheil, *Theoretical and numerical study of evaporation effects in spray flamelet model*, in *Experiments and Numerical Simulations of Turbulent Combustion of Diluted Sprays*, B. Merci and E. Gutheil, eds., Springer, 2014, pp. 79–106.

[34] D. Maionchi and F. Fachini, *Simple spray–flamelet model: Influence of ambient temperature and fuel concentration, vaporisation source and fuel injection position*, Combust. Theory and Modelling 17 (2013), pp. 522–542.

[35] F.A. Williams, *Combustion Theory*, Benjamin Cummings, Menlo Park, CA, 1985.

[36] A. Liñán, *The asymptotic structure of counterflow diffusion flames for large activation energies*, Acta Astronautica 1 (1974), pp. 1007–1039.

[37] T. Poinsot and D. Veynante, *Theoretical and Numerical Combustion, Third Edition*, 2012.

[38] K. Seshadri and N. Peters, *Simulation of a turbulent spray flame using coupled pdf gas phase and spray flamelet modeling*, Combust. Flame 73 (1988), pp. 24–44.

[39] M. Maxey and J. Riley, *Equation of motion for a small rigid sphere in a non uniform flow*, Phys. Fluids 26(4) (1983), pp. 2883–2889.

[40] R.W. Bilger, S.H. Starner, and R.J. Kee, *On reduced mechanisms for methane-air combustion in nonpremixed flames*, Combust. Flame 80 (1990), pp. 135–149.

[41] J. Urzay, D. Martìnez-Ruiz, A.L. Sánchez, A. Liñán, and F.A. Williams, *Flamelet structures in spray ignition*, Annual Research Briefs, Center for Turbulence Research, Stanford (2014), pp. 107–122.

[42] B. Franzelli, E. Riber, M. Sanjosé, and T. Poinsot, *A two-step chemical scheme for large eddy simulation of kerosene-air flames*, Combust. Flame 157 (2010), pp. 1364–1373.

[43] F. Laurent and M. Massot, *Multi-fluid modeling of laminar poly-dispersed spray flames: origin, assumptions and comparison of the sectional and sampling methods*, Combust. Theory and Modelling 5 (2001), pp. 537–572.

[44] D. Kah, F. Laurent, L. Fréret, S. de Chaisemartin, R. Fox, J. Reveillon, and M. Massot, *Eulerian quadrature-based moment models for dilute polydisperse evaporating sprays*, Flow, Turb. and Combustion 85 (2010), pp. 649–676.

[45] J. Ferry and S. Balachandar, *A fast Eulerian method for disperse two-phase flow*, Int. J. Multiphase Flow 27 (2001), pp. 1199–1226.

[46] H. Pitsch and N. Peters, *A consistent flamelet formulation for non-premixed combustion considering differential diffusion effects*, Combust. Flame 114 (1998), pp. 26–40.

Appendix A. One-dimensional counterflow spray flames equations

A.1 *Modeling approach*

The counterflow spray flame equations are solved on the axis of symmetry $x_2 = 0$, from the fuel to the oxidizer side. To focus on the coupling between mass transfer, mixing, and reaction, the following simplifying assumptions are invoked for the numerical solution of the governing equations:

- A constant strain rate is assumed [19, 20]: $u_1 = -ax_1$ and $u_2 = ax_2$.
- For evaporation, a simplified d^2-model is considered by fixing the droplet temperature[1] $T_l = T_b$, where T_b is the boiling temperature of the fuel species. Consequently, the evaporation model writes [6]:

$$\dot{m} = 2\pi n_l d\rho D \ln\left(\frac{c_p}{L_v}(T - T_l)\right)\mathcal{H}(T - T_l)\ , \tag{A1}$$

$$q = L_v\ , \tag{A2}$$

  where $\mathcal{H}(\cdot)$ is the Heaviside function. The liquid fuel properties for kerosene are $T_b = 478$ K and $L_v = 289.9$ kJ/kg.
- The liquid velocity is assumed to be the same as that of the gas velocity. This assumption is valid for small Stokes-number droplets based on the gaseous flow strain rate $\mathrm{St}_d = a\tau_d$ (where $\tau_d = \rho_l d^2/(18\mu)$ is the particle relaxation time [39]). It has to be noted that such a system cannot capture droplets with a Stokes number greater than 1/4 that could potentially cross the stagnation and exhibit velocity reversal. Capturing such a behaviour should be handled by using more velocity moments [44] or by introducing additional droplet classes [6].
- Constant thermo-diffusive properties[2] with $\rho D = 2 \times 10^{-5}$ kg/(m s) and $c_p = 1300$ J/(kg K).

With these assumptions, the system of equations that is solved in physical space takes the following form:

$$-ax\frac{\mathrm{d}Y_k}{\mathrm{d}x} = \rho D\frac{\mathrm{d}^2Y_k}{\mathrm{d}x^2} + \dot{m}(\delta_{kF} - 1) + \dot{\omega}_k\ , \tag{A3a}$$

$$-ax\frac{\mathrm{d}T}{\mathrm{d}x} = \rho D\frac{\mathrm{d}^2T}{\mathrm{d}x^2} + \dot{m}\left(T_l - T - \frac{L_v}{c_p}\right) + \dot{\omega}_T\ , \tag{A3b}$$

$$-ax\frac{\mathrm{d}Z_l}{\mathrm{d}x} = -\dot{m}(Z_l + 1)\ , \tag{A3c}$$

$$-ax\frac{\mathrm{d}m_d}{\mathrm{d}x} = -\dot{m}\frac{\rho}{n_l}\ , \tag{A3d}$$

where the density is calculated from the species mass fractions, the temperature, and the constant thermodynamic pressure using the ideal gas law.

[1] The assumption of constant liquid temperature is not valid for real applications [3], the transient heating time being of primary importance. However, since the main concern about the definition of a composition space is the effect of the vaporization rate, this assumption has no consequence on the suitability of our methodology when liquid temperature variations are taken into account.

[2] It is worth mentioning that this assumption could be relaxed to take into account density effects on the flow structure, by using the Howarth-Dorodnitzyn approximation under the classical boundary layer approximation [35].

In this configuration, the equation for η is:

$$-ax\frac{\mathrm{d}\eta}{\mathrm{d}x} = \mathrm{sgn}(u_\eta)\sqrt{\left(-ax\frac{\mathrm{d}Z_g}{\mathrm{d}x}\right)^2 + \left(-ax\frac{\mathrm{d}Z_l}{\mathrm{d}x}\right)^2} \,. \tag{A4}$$

To construct a monotonic composition space, we thus impose:

$$-ax\frac{\mathrm{d}\eta}{\mathrm{d}x} = \mathrm{sgn}(-ax)\sqrt{\left(-ax\frac{\mathrm{d}Z_g}{\mathrm{d}x}\right)^2 + \left(-ax\frac{\mathrm{d}Z_l}{\mathrm{d}x}\right)^2} \,. \tag{A5}$$

The corresponding spray-flamelet system in composition space reads as:

$$\Xi_\eta^\dagger\frac{\mathrm{d}Y_k}{\mathrm{d}\eta} = \frac{\rho\chi_\eta}{2}\frac{\mathrm{d}^2Y_k}{\mathrm{d}\eta^2} + (\delta_{kF} - Y_k)\dot{m} + \dot{\omega}_k \,, \tag{A6a}$$

$$\Xi_\eta^\dagger\frac{\mathrm{d}T}{\mathrm{d}\eta} = \frac{\rho\chi_\eta}{2}\frac{\mathrm{d}^2T}{\mathrm{d}\eta^2} + \dot{m}\left(T_l - T - \frac{L_v}{c_p}\right) + \dot{\omega}_T \,, \tag{A6b}$$

$$\Xi_\eta\frac{\mathrm{d}Z_l}{\mathrm{d}\eta} = -\dot{m}\,(1 + Z_l) \,, \tag{A6c}$$

$$\Xi_\eta\frac{\mathrm{d}m_d}{\mathrm{d}\eta} = -\dot{m}\frac{\rho}{n_l} \,, \tag{A6d}$$

with

$$\Xi_\eta = \left[1 - 2\mathcal{H}\left(Z_g - \frac{Z_g^*}{2}\right)\right]\left\{\left(\frac{\mathrm{d}Z_g}{\mathrm{d}\eta}\frac{\rho D}{2}\frac{\mathrm{d}}{\mathrm{d}\eta}\left(\frac{\chi_\eta}{2D}\right) + \frac{\rho\chi_\eta}{2}\frac{\mathrm{d}^2Z_g}{\mathrm{d}\eta^2} + (1 - Z_g)\dot{m}\right)^2 + (\dot{m}\,(1 + Z_l))^2\right\}^{1/2} \,, \tag{A7a}$$

$$\Xi_\eta^\dagger = \Xi_\eta - \frac{\rho D}{2}\frac{\mathrm{d}}{\mathrm{d}\eta}\left(\frac{\chi_\eta}{2D}\right) \,, \tag{A7b}$$

and $\left[1 - 2\mathcal{H}\left(Z_g - Z_g^*/2\right)\right]$ is introduced to model $\mathrm{sgn}(u_\eta) = -\,\mathrm{sgn}(x)$ as shown in App. B. It is noted that $\Xi_\eta^\dagger$ is equal to zero on the gas side.

For the limit of small Stokes numbers, all droplets evaporate before crossing the stagnation plane, which corresponds to the region of negative velocity. The assumption could be violated for larger droplets if their Stokes number $\mathrm{St}_d = a\tau_p$ is higher than 1/4 [6], requiring a closure model that accounts for the slip velocity between the gas and liquid phase. However, it is also noted that even droplets with a high Stokes number could evaporate before reaching the stagnation plane. This is likely to occur for hydrocarbon fuels, for which the latent heat of vaporization is small compared to those fuels that are commonly used to study droplet crossings [6, 27]. Moreover, a closure model accounting for effects of the slip velocity on the flame structure is proposed in App. D, under the assumption of small St_d. For high values of St_d, the transport equation for the liquid velocity (Eq. (24f)) may also be added to the system. As result of the zero-slip velocity assumption, that is $u_i = u_{l,i}$, χ_η is the only unclosed term in the spray-flamelet equations (A6). This term is directly evaluated from the x-space solution in Sec. 5.1. Subsequently, this approximation is relaxed in Secs. 5.2 and 5.3 and a model for the scalar dissipation rate is developed in App. C.

A.2 *Numerical method*

To solve Eqs. (A3) and (A6) in their respective physical and effective composition spaces, four numerical ingredients are used:

- An adaptive mesh refinement method is used based on the gradients of η in physical space.
- Diffusive operators, i.e. second order derivatives, are discretized using a central finite difference scheme. Considering a non-uniform mesh spacing of elements Δx_i, the second order derivative of a quantity Φ at the location i is:

$$\left.\frac{\mathrm{d}^2\Phi}{\mathrm{d}x^2}\right|_i \approx \frac{\Delta x_{i-1}\Phi_{i+1} - (\Delta x_{i-1} + \Delta x_i)\Phi_i + \Delta x_i \Phi_{i-1}}{\Delta x_{i-1}\Delta x_i \dfrac{\Delta x_{i-1} + \Delta x_i}{2}}. \tag{A8}$$

- Convective operators, i.e. first order derivatives, are discretized using an upwind finite difference scheme:

$$U\left.\frac{\mathrm{d}\Phi}{\mathrm{d}x}\right|_i \approx \max(0, U_i)\frac{\Phi_i - \Phi_{i-1}}{\Delta x_{i-1}} + \min(0, U_i)\frac{\Phi_{i+1} - \Phi_i}{\Delta x_i}. \tag{A9}$$

- Steady-state is reached through a pseudo-time advancement with explicit Euler scheme. Considering τ as the increment of the pseudo-time variable and n as the time iteration:

$$\left.\frac{\mathrm{d}\Phi}{\mathrm{d}\tau}\right|_i^n \approx \frac{\Phi_i^{n+1} - \Phi_i^n}{\tau}. \tag{A10}$$

Appendix B. Analytical solution for Z_g, Z_l and η

The analytical profiles for the gaseous and liquid-to-gas mass ratio in η-space are here derived for the 1D laminar counterflow flame, described in App. A (Eqs. (A3)). To obtain a closed-form solution, the following assumptions are introduced:

- Consistent with the modeling of the scalar dissipation rate of gaseous flames [24], a constant density $\rho = \rho^0$ is considered so that $D = D^0$.
- Starting from a d^2-evaporation law, for which the evaporation rate is proportional to the droplet diameter (that is $d \propto Z_l^{1/3}$):

$$\dot{m} = \frac{\rho^0}{\tau_v}(Z_l^0)^{2/3} Z_l^{1/3}\ , \tag{B1}$$

a linearized evaporation model at Z_l^0 is derived:

$$\frac{\dot{m}}{a\rho^0} = \frac{1}{3\mathrm{St}_v}\left(2Z_l^0 + Z_l\right) = \frac{1}{\alpha}\left(2Z_l^0 + Z_l\right)\ , \tag{B2}$$

where $\alpha = 3\mathrm{St}_v$, $\mathrm{St}_v = a\tau_v$ is the evaporation Stokes number, and τ_v is the constant evaporation time.

The equations for the liquid-to-gas mass ratio and the gaseous mixture fraction, Eqs. (1d) and (5a), are then given in non-dimensional form as:

$$\xi \frac{\mathrm{d}Z_l}{\mathrm{d}\xi} = \frac{1}{\alpha}\left(2Z_l^0 + Z_l\right)(1 + Z_l)\,, \tag{B3a}$$

$$\frac{\mathrm{d}^2 Z_g}{\mathrm{d}\xi^2} + 2\xi \frac{\mathrm{d}Z_g}{\mathrm{d}\xi} = \frac{2}{\alpha}\left(2Z_l^0 + Z_l\right)(Z_g - 1)\,, \tag{B3b}$$

where $\xi = x/\delta_D$, and $\delta_D = \sqrt{2D^0/a}$ is the diffusion layer thickness. Profiles of mixture-fraction distributions are schematically illustrated in Fig. B1.

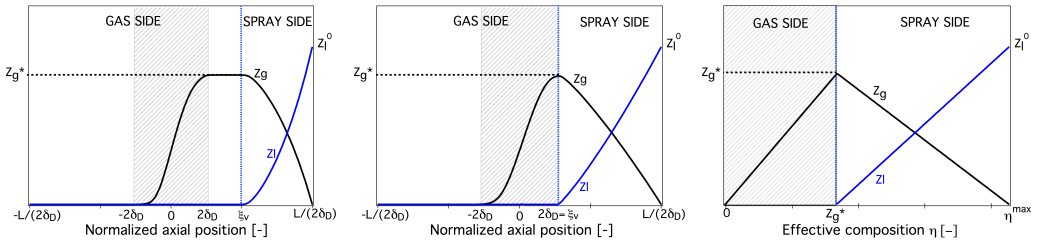

(a) Physical space; small vaporization time τ_v. (b) Physical space; large vaporization time τ_v. (c) Effective composition space; large vaporization time τ_v.

Figure B1.: Schematic representation of gaseous mixture fraction and liquid-to-gas mass ratio profiles in physical space for (a) small vaporization times τ_v and (b) large values of τ_v (corresponding to the limit of the present model), and (c) representation in effective composition space. The gray zone identifies the diffusion layer. The blue vertical line separates the gas side from the spray side.

An analytic solution for Z_l can be obtained by solving Eq. (B3a); however, we were not able to find a closed-form solution for Eq. (B3b). An analytical solution can be obtained for the asymptotic limit in which effects of evaporation and species diffusion are spatially separated. For this case, the gaseous mixture fraction increases on the spray side until reaching its maximum; once the evaporation is completed ($Z_l = 0$), the diffusion becomes relevant and the spatial evolution of Z_g is described by the purely gaseous mixture-fraction equation (see Figs. B1(a) and B1(b)). It is important to recognize that this zonal separation is different from a pre-vaporized spray flame, in which liquid fuel is evaporated before diffusion and combustion occur, and combustion is confined to the gaseous side. The present formulation is not restricted to this special case and allows for the spatial superposition of evaporation and combustion. With this, the flame can be separated into two regions:

(1) *Spray side for $\xi > \xi_v$:* The liquid volume fraction starts evaporating close to the injection $\xi = L/(2\delta_D)$ and completely disappears at $\xi = \xi_v$. The main contribution in this region is assumed to arise from the evaporation, so that contributions from diffusion in the Z_g-equation can be neglected:

$$\xi \frac{\mathrm{d}Z_l}{\mathrm{d}\xi} = \frac{1}{\alpha}\left(2Z_l^0 + Z_l\right)(1 + Z_l)\,, \tag{B4a}$$

$$\xi \frac{\mathrm{d}Z_g}{\mathrm{d}\xi} = \frac{1}{\alpha}\left(2Z_l^0 + Z_l\right)(Z_g - 1)\,. \tag{B4b}$$

The analytic solutions for Z_l and Z_g can be written as:

$$Z_l(\xi) = -2Z_l^0 \frac{1-(\xi/\xi_v)^\beta}{2Z_l^0-(\xi/\xi_v)^\beta} \,, \tag{B5a}$$

$$Z_g(\xi) = -\frac{1-2Z_l^0}{1+Z_l^0} \frac{1}{1-2Z_l^0(\xi/\xi_v)^{-\beta}} + 1 \,, \tag{B5b}$$

where $\beta = (2Z_l^0 - 1)/\alpha$, and the value for ξ_v is obtained by imposing the boundary condition $Z_l(L/(2\delta_D)) = Z_l^0$ in Eq. (B5a):

$$\xi_v = \frac{L}{2\delta_D} \left(\frac{3}{2(1+Z_l^0)} \right)^{1/\beta} . \tag{B6}$$

The extension of this region depends on the evaporation time τ_v through the parameter β: increasing the evaporation time leads to a broadening of the evaporation zone, and the limiting case of this model is represented in Figs. B1(b) and B1(c).

The maximum value of the gaseous mixture fraction Z_g^*, found at $\xi = \xi_v$, is calculated using Eqs. (B5) and (B6):

$$Z_g^* = \frac{Z_l^0}{(1+Z_l^0)} \equiv \frac{1}{K_1} \,. \tag{B7}$$

From Eqs. (B5) a relation between Z_g and Z_l can be derived for the evaporation region:

$$Z_l = Z_l^0 - (1+Z_l^0) Z_g \,, \qquad \frac{\mathrm{d}Z_l}{\mathrm{d}\xi} = -\frac{K_1}{(K_1-1)} \frac{\mathrm{d}Z_g}{\mathrm{d}\xi} \,. \tag{B8}$$

(2) *Gas side for $\xi \leq \xi_v$:* In this region, the liquid volume fraction is zero and the expression for Z_g reduces to the classical equation for gaseous flames.

$$Z_l = 0 \,, \tag{B9a}$$

$$Z_g = \frac{Z_g^*}{2} \left(1 + \mathrm{erf}(\xi)\right) \,, \tag{B9b}$$

where the last equation is obtained by setting the right-hand-side of Eq. (B3b) to zero and using the boundary conditions $Z_g(-\infty) = 0$ and $Z_g(\xi_v) = Z_g^{+\infty}$. It is noted that Z_g asymptotically reaches the value Z_g^* at $\xi = \xi_v$, since our model implies $\xi_v \geq 2\delta_D$. From Eq. (B9b), it is found that the stagnation point required to evaluate the function $\mathrm{sgn}(x) = \mathrm{sgn}(\xi)$ corresponds to $Z_g = Z_g^*/2$.

The analytic formulation for η is then obtained by combining Eqs. (B5) and (B9):

$$\eta(\xi) = \begin{cases} \int_{-\infty}^{\xi} \sqrt{\left(\frac{\mathrm{d}Z_g}{\mathrm{d}\xi}\right)^2}\mathrm{d}\xi = \frac{Z_g^*}{2}\left(1+\mathrm{erf}(\xi)\right) & \text{if } \xi \le \xi_v \,, \\ Z_g^* + \int_{\xi_v}^{\xi} \sqrt{\left(\frac{\mathrm{d}Z_g}{\mathrm{d}\xi}\right)^2 + \left(\frac{\mathrm{d}Z_l}{\mathrm{d}\xi}\right)^2}\mathrm{d}\xi = Z_g^* + K_2 Z_l^0 - K_2(1+Z_l^0)Z_g(\xi) & \text{if } \xi > \xi_v \,, \end{cases} \tag{B10}$$

where $K_2 = \sqrt{(1-Z_g^*)^2+1}$. Through the spatial separation of the evaporation and diffusion regions of the flame, it can be seen from Eq. (B10) that η is only a function of Z_l^0 and St_v. The maximum value of the effective mixture fraction is evaluated as:

$$\eta^{\max} = \eta(\xi = L/(2\delta_D)) = \frac{Z_l^0}{1+Z_l^0}\left(1+\sqrt{2+2Z_l^0+\left(Z_l^0\right)^2}\right) \,, \tag{B11}$$

which is only a function of the liquid mass fraction at injection.

Invoking the linear dependence of liquid and gaseous mixture fractions on the effective composition variable (see Fig. B1(c)), Z_g and Z_l can be written as functions of η:

$$Z_g(\eta) = \begin{cases} \eta & \text{if } \eta \le Z_g^* \,, \\ \dfrac{\eta-\eta^{\max}}{1-\eta^{\max}/Z_g^*} & \text{if } \eta > Z_g^* \,, \end{cases} \tag{B12}$$

and

$$Z_l(\eta) = \begin{cases} 0 & \text{if } \eta \le Z_g^* \,, \\ Z_l^0\left(\dfrac{\eta-Z_g^*}{\eta^{\max}-Z_g^*}\right) & \text{if } \eta > Z_g^* \,. \end{cases} \tag{B13}$$

As discussed in Sec. 4.2, the validity of the analytical solution relies on the assumption that mixing and evaporation occur in two distinct regions.

Appendix C. Closure model for the scalar dissipation

A closure model for the scalar dissipation rate χ_η can be derived using the analytic expressions for Z_g and Z_l that were derived in the previous section. For this, we decompose Eq. (25d) into liquid and gaseous contributions:

$$\chi_\eta = \chi_{Z_g} + \chi_{Z_l} \,, \tag{C1}$$

and corresponding expressions directly follow from the definition of the effective composition variable.

The scalar dissipation of the liquid-to-gas mass ratio is evaluated from the analytic solution of Z_l (Eq. B5a):

$$\chi_{Z_l} = K_3(2Z_l^0+Z_l)^{2+2/\beta}(1+Z_l)^{2-2/\beta} \,, \tag{C2}$$

where $K_3 = (2Z_l^0)^{-2/\beta} \frac{8D^0}{\alpha^2 L^2} \left[\frac{2(1+Z_l^0)}{3}\right]^{2/\beta}$.

To derive the gaseous scalar dissipation rate χ_{Z_g}, the diffusion and the evaporation contributions are considered separately: $\chi_{Z_g} = \chi_{Z_g^{\text{evap}}} + \chi_{Z_g^{\text{mix}}}$. The scalar dissipation of the gaseous mixture fraction on the gas side in the absence of liquid volume fraction, is given in analogy with a purely gaseous flame (Eq. B9b):

$$\chi_{Z_g}^{\text{mix}} = \frac{a(Z_g^*)^2}{\pi} \exp\left(-2\left[\text{erf}^{-1}\left(\frac{2Z_g}{Z_g^*} - 1\right)\right]^2\right) . \tag{C3}$$

The scalar dissipation of the gaseous mixture fraction on the spray side is obtained from Eq. (B5b):

$$\chi_{Z_g}^{\text{evap}} = K_3(2Z_l^0 + Z_l)^{2+2/\beta}(1 + Z_l)^{-2/\beta}(1 - Z_g)^2. \tag{C4}$$

The individual contributions are combined to describe the dissipation rate of the effective composition variable in the gaseous and liquid regions of the flame:

$$\chi_\eta = \begin{cases} \chi_{Z_g}^{\text{mix}} & \text{if } \eta \le Z_g^* \ , \\ \chi_{Z_g}^{\text{evap}} + \chi_{Z_l} & \text{if } \eta > Z_g^* \ . \end{cases} \tag{C5}$$

The analytical closure is compared to the χ_η-profile from the solution in physical space for the case with $\tau_v = 0.005$ s from Sec. 5.2. Results from this comparison are shown in Fig. C1. For this case, diffusion and evaporation occur in two distinct regions and the analytical closure model is able to reproduce χ_η in both regions. Extending the closure model to more general cases for which evaporation and diffusion are not separated is feasible for instance by directly evaluating χ_η from the simulation or by combining the contributions from $\chi_{Z_g}^{\text{mix}}$, $\chi_{Z_g}^{\text{evap}}$ and χ_{Z_l} in the region where diffusion and evaporation occur simultaneously. This zone may be identified by evaluating the non-linear behavior of Z_g in the η-space as discussed in Sec. 4.

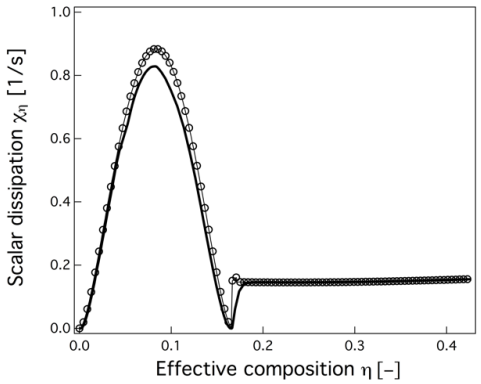

Figure C1.: Effective composition dissipation rate as a function of η. Result from the physical solution for $\tau_v = 0.005$ s in Sec. 5.2 (line) is compared to the analytical model (symbols).

Appendix D. Analytic model for slip velocity

The assumptions of App. A are here retained to derive a model for the slip velocity contribution $\Psi_d\,[\phi]$ for a counterflow spray flame. For this, we follow the work of Ferry and Balachandar [45] and evaluate the velocity of the liquid phase from the gaseous velocity:

$$u_{l,i} = u_i - \frac{Du_i}{Dt}\tau_d + \mathcal{O}(\tau_d^2)\ , \tag{D1}$$

where $\frac{D}{Dt}$ is the material derivative of the gas phase. Under the assumption of constant strain rate and potential flow solution [11, 19], the liquid velocity can be written as:

$$u_{l,i} = u_i\,(1 - \mathrm{St}_d) + \mathcal{O}(\mathrm{St}_d^2)\ . \tag{D2}$$

By considering the limit of small Stokes number, higher-order terms are truncated, and the following expression for the slip-velocity contribution is obtained:

$$\Psi_d\,[\phi] = \rho u \mathrm{St}_d \frac{\mathrm{d}\eta}{\mathrm{d}x}\frac{\mathrm{d}\phi}{\mathrm{d}\eta} - \frac{2}{3}\frac{\phi}{Z_l}\frac{\mathrm{St}_d}{1-\mathrm{St}_d}\dot{m}\ . \tag{D3}$$

This closure model can be used to take into account the effect of a slip velocity between liquid and gaseous phases on the flame structure.

The flame structure defined by the 1D spray-flamelet formulation given in Eqs. (24) depends on the liquid and gaseous velocities through the quantities Ξ_η and Ψ_d. However, when using Eq. (D2), the dependence on the velocity of both phases is eliminated and only the dependence on the droplet Stokes number is retained:

$$\Xi_\eta^\dagger \frac{\mathrm{d}Y_k}{\mathrm{d}\eta} = \frac{1}{2}\rho\chi_\eta\frac{\mathrm{d}^2Y_k}{\mathrm{d}\eta^2} + (\delta_{kF} - Y_k)\dot{m} + \dot{\omega}_k\ , \tag{D4a}$$

$$\Xi_\eta^\dagger \frac{\mathrm{d}T}{\mathrm{d}\eta} = \frac{1}{2}\rho\chi_\eta\frac{\mathrm{d}^2T}{\mathrm{d}\eta^2} + \dot{\omega}_T + \dot{m}\left(T_l - T - \frac{q}{c_p}\right)\ , \tag{D4b}$$

$$\Xi_\eta(1-\mathrm{St}_d)\frac{\mathrm{d}Z_l}{\mathrm{d}\eta} = -\frac{2\mathrm{St}_d}{3(1-\mathrm{St}_d)}\dot{m} - \dot{m}\,(1+Z_l)\ , \tag{D4c}$$

$$\Xi_\eta(1-\mathrm{St}_d)\frac{\mathrm{d}m_d}{\mathrm{d}\eta} = -\frac{2\mathrm{St}_d}{3(1-\mathrm{St}_d)Z_l}\dot{m}\frac{n_l}{\rho} - \dot{m}\frac{\rho}{m_d}\ . \tag{D4d}$$

In the limit of small Stokes number $\mathrm{St}_d \to 0$, the liquid and gaseous velocities are identical, so that the spray-flamelet formulation simplifies to the system given by Eqs. (A6).

Appendix E. Non-unity Lewis number flows

In the present work, we invoked the unity Lewis assumption, which is a classical assumption for the development of flamelet methods. However it is well known that hydrocarbon liquid fuels, such as dodecane or kerosene, have a Lewis number above 2. Here we kept the unity Lewis number assumption for the sake of simplicity and clarity, since the focus of the work is on the formulation of an effective composition

space. Nevertheless, extending this formulation to a non-unity Lewis-number systems is possible. For this, we recall the equation of the gaseous mixture fraction, but in the case of non-unity Lewis Number:

$$\rho u_i \frac{\partial Z_g}{\partial x_i} = \frac{\partial}{\partial x_i}\left(\rho D \frac{\partial Z_g}{\partial x_i}\right) + (1 - Z_g)\dot{m} \, , \\ + \frac{W_F}{n_{C,F} W_C} \sum_{k=1}^{N_s} \frac{n_{C,k} W_C}{W_k} \frac{\partial}{\partial x_i}\left(\rho (D_k - D) \frac{\partial Y_k}{\partial x_i}\right) \, , \tag{E1}$$

where D is a mean diffusion coefficient and D_k is the diffusion coefficient of species k. As shown for instance in [28], such a definition of the mixture fraction is not monotonic even for gaseous flames, and thus can not be used as a proper composition space variable. However, if we look at the purely gaseous case, and use our composition space variable η:

$$\frac{\mathrm{d}\eta}{\mathrm{d}t} = \mathrm{sgn}\left(\frac{\mathrm{d}\eta}{\mathrm{d}t}\right) \sqrt{\left(\frac{\mathrm{d}Z_g}{\mathrm{d}t}\right)^2} \, , \tag{E2}$$

any variation of Z_g will lead to a monotonic variation of η on either fuel or oxidizer sides of the flow. Consequently, our η-space formulation can handle non-unity Lewis number assumption.

Another possible solution is to use the strategy proposed by Pitsch and Peters [46], who introduces a mixture fraction that is not linked to the species in the flow, and is by definition a passive scalar. This way, even if this formulation cannot be linked to physical quantities, it can be used as a composition space variable.